Major modification of sediment routing by a large Mass Transport Deposit in the Gulf of Lions (Western Mediterranean)

B. Dennielou, Isabelle Jégou, Laurence Droz, Gwenael Jouet, Antonio Cattaneo, Serge S. Berné, Daniel Aslanian, Benoît Loubrieu, Marina Rabineau, Sylvain Bermell

Major modification of sediment routing by a large Mass Transport Deposit in the Gulf of Lions (Western Mediterranean)

B. Dennielou[1], I. Jégou[2, 1], L. Droz[2], G. Jouet[1], A. Cattaneo[1], S. Berné[3], D. Aslanian[1], B. Loubrieu[1], M. Rabineau[2], Sylvain Bermell[1]

1- IFREMER, Centre de Brest, Unité de Recherche Géosciences Marines, 29280 Plouzané, France

2- UMR 6538 Géosciences Océan, Université de Brest, UBO, Institut Universitaire Européen de la Mer, France

3-Université de Perpignan, Laboratoire CEFREM, UMR-CNRS 5110, 52 Av. P. Alduy, 66860 Perpignan, France

Keywords

Gulf of Lions, Ebro margin, Sediment routing, Rhone deep-sea fan, Canyon, Mass transport deposit, Turbidite

Highlights

- Submarine Mass Transport Deposits can radically modify sediment routing pathways on the continental slope and rise.
- Large Mass Transport Deposits (160 km^3) can be obscured on the seabed where sedimentation rate is high.

Abstract

In the Gulf of Lions (Western Mediterranean), the emplacement of a large (160 km^3) Mass Transport Deposit, the Rhone Western Mass Transport Deposit (RWMTD), at the base of slope, aside the Rhone deep-sea fan between 1800 and 2700 m water depth, resulted in a major modification of the sediment routing by clogging a drainage network and blocking at the base of slope sediments that were previously routed into the Valencia channel and the Balearic abyssal plain. The RWMTD was sourced from sediments of the western flank of the Rhone upper fan and the adjacent base of slope. The mass transport deposit is characterized by a transparent seismic facies and sediment cores show that it is composed of a stiff laminated muddy lithofacies characteristic of the Rhone fan turbidites with marked contorted beds indicative of remoulding. AMS radiocarbon dating shows that the RWMTD was emplaced between 19.9-21.5 ka cal. BP. It is coeval, within dating uncertainties, with the emplacement of a megaturbidite in the Balearic Abyssal Plain and immediately predates a major avulsion of the Rhone turbidite channel that led to the emplacement of an avulsion lobe (the neofan) on top of the RWMTD. It is not possible to affirm a genetic link between these three major gravity events but one can argue that they share a common forcing in relation with massive turbiditic accumulation during the last sea-level lowstand at the end of the Last Glacial Maximum. This study outlines the importance of mass transport deposits in the building of turbidite systems and, more generally, the major control of mass wasting on the routing and dispersal of sediments across continental margins.

1. Introduction

Besides geohazard and societal issues, slope failures and mass transport deposits play a significant role in the long-term evolution of continental margins because they involve

51 the displacement of very important volumes of sediments and significantly modify the
52 margins morphology and the submarine sediment dispersal pattern (Huppertz et al.,
53 2010; Joanne et al., 2010; Kawamura et al., 2010; Mulder, 2011; Shipp et al., 2011).
54 Furthermore, mass transport deposits may represent up to 10-20% of stratigraphic
55 sequences on continental margins (McHugh et al., 1996; Mulder, 2011; Weimer, 1989).
56 They can play a significant role in the movement and transfer of sediment at river mouth
57 deltas or canyon heads at hourly or yearly time scales (Biscara et al., 2012; Clare et al.,
58 2016 ; Kelner et al., 2014; Mazières et al., 2014; Obelcz et al., 2017; Smith et al., 2007),
59 but also at geologic time scales on canyons and whole margin development (Micallef et
60 al., 2012; Sultan et al., 2007). This is particularly the case for large mass transport
61 deposits that instantaneously redistribute huge volumes of sediment, in the order of
62 several km^3. These are dominantly emplaced on slopes receiving massive sediment
63 input such as glaciated margins (Bryn et al., 2005; Gales et al., 2014; Imbo et al., 2003;
64 Jansen et al., 1987; Lee, 2009; Piper et al., 2003) or deltaic margins during periods of low
65 sea level (Droz and Bellaiche, 1985; Garziglia et al., 2008; Nelson et al., 2011; Piper et al.,
66 1997; Weimer, 1989). They also represent a significant sediment input into abyssal
67 plains in the form of megabeds, particularly in the Mediterranean Sea (Cita and Aloisi,
68 2000; Reeder et al., 2000; Rothwell et al., 1998; San Pedro et al., 2017)}.
69 In the Gulf of Lions (GoL) (Western Mediterranean) (Fig. 1), the Rhone deep-sea fan
70 developed since the Pliocene in a complex geologic setting characterized by a
71 continental slope dissected by several shifting canyons (Berné et al., 1999; Bourcart,
72 1960; Torres et al., 1995), salt tectonics (dos Reis et al., 2005; Droz, 1983; Gaullier,
73 1993; Le Cann, 1987) and canyon and open slope mass wasting (Sultan et al., 2007).
74 Mass transport deposits on the Rhone fan have long been recognized as major features
75 with high impact on the Late Quaternary fan growth (Droz and Bellaiche, 1985; Gaullier

et al., 1998). We present a new detailed mapping of the superficial Rhone Western mass transport deposit (RWMTD) based on a synthesis and reinterpretation of bathymetric and seismic data acquired during several oceanographic campaigns since 1997, and new litho-facies and chronological data from three sediment cores that penetrated the deposits. In addition to considerations on the sedimentary source and trigger mechanisms, the aim of this study is to outline the role played by the emplacement of the RWMTD at the base of slope in the evolution of sediment routing patterns in the western part of the GoL from the upper slope to the Balearic Abyssal Plain within the context of sea-level fluctuations since the Last Glacial Maximum (LGM).

2. Geological background

2.1. Sedimentary setting

Following the reflooding of the basin, after a major sea level drop of the Mediterranean Sea during the Messinian (1500 m according to Hsü et al. (1973)), 3 km of prograding and aggrading sediments were deposited throughout the Plio-Quaternary to reach the present day margin morphology (Leroux et al., 2014; Lofi et al., 2003). Following the Mid-Pleistocene transition (1,250- 700 ka BP; (Clark et al., 2006)), sediment accumulation on the GoL margin increased by two-fold as a result of the increased magnitude of global sea-level changes (Leroux et al., 2017). During the Late Pleistocene, the evolution of the margin and canyons was driven by sea-level fluctuations and thermal subsidence, in the order of 250 $m.Ma^{-1}$, creating accommodation prone to the deposition of sediments (Rabineau et al., 2006; Rabineau et al., 2014). During sea-level falls thick forced-regressive sequences developed (Bassetti et al., 2008; Rabineau et al., 2005; Rabineau et al., 1998; Tesson and Gensous, 1998; Torres et al., 1995) bounded on the slope by condensed intervals, deposited during highstands (Sierro et al., 2009).

During this period of time the evolution of the deep GoL was also controlled by syn-sedimentary salt tectonics. Gravitational gliding and spreading over the Messinian detachment salt level (dos Reis et al., 2005) developed at the mid to lower slope with basinward-dipping active and buried listric faults parallel to sub-parallel to the shelf break (dos Reis et al., 2005) (Fig. 2).

2.2. Sediment routing

In the GoL the main source of sediment is the Rhône River (Pont et al., 2002). Through geological times, sediment dispersal at the mouth of rivers was controlled by sea level fluctuations and the synchronous migration of the shoreline. During periods of low sea level (glacials), the seaward migration of the shoreline moved the sediment depocenters onto to the outer shelf and a significant amount of sediment was routed into the canyons, as evidenced by preserved marked sinuous incisions at some canyons (Baztan et al., 2005; Mauffrey et al., 2015). Numerous canyons dissect the shelf break. In the western part of the GoL, eight canyons, Cap de Creus to Marti canyons, coalesce down slope but do not show a connection with the Valencia channel (Amblas et al., 2006; Baztan et al., 2005; Berné et al., 2004). In the central adjacent part the Petit-Rhone canyon shows a sinuous pattern and is prolonged by the Rhone turbidite system (Droz et al., 2006) (Fig. 1). The developed sinuous channel network of the Rhone turbidite system (Droz et al., 2006) shows that during lowstands a large amount of sediment was efficiently exported as deep as 2800 m water depth and possibly into the Balearic Abyssal Plain. To the west, the sediments were likely funneled into the Sète canyon network and deposited at the base of slope where the canyons morphology abruptly smoothens (Fig. 1). The same configuration applies for La Fonera and Clots del Puget canyons. In comparison, to the southwest, on the south Catalan margin canyons coalesce

and extend beyond the base of slope to finally vanish into the Valencia Fan at the northernmost part of the Algerian–Balearic Abyssal plain (Amblas et al., 2011; Maldonado et al., 1985) (Fig. 1). One particularly noteworthy event during the last sea-level rise on the Ebro margin was the emplacement of the Big'95 mass transport deposit that caused a sudden change in sedimentation style in the upper segment of the Valencia drainage network, with a significant decrease in sediment transport and incision capacity (Amblas et al., 2011).

2.3. Turbidite systems

Two thick turbidite systems lie at the base of slope in the GoL, the Rhone turbidite system in the central part of the GoL and the Pyreneo-Languedocian Sedimentary Ridge to the west as shown on the Quaternary isopach map (dos Reis et al., 2005). Smaller turbiditic sedimentary ridges lie at the right hand side of the La Fonera and Clots del Puget canyons (Fig. 1). All these turbidite systems consist of terrigenous sediment, starved during the Holocene highstand, and displaying high sedimentation rates during the LGM lowstand (Beaudouin et al., 2004; Jallet and Giresse, 2005; Lombo Tombo et al., 2015; Melki et al., 2009). The Rhone turbidite system, the largest turbidite system in terms of thickness and area in the GoL and in the western Mediterranean Sea, lies in the prolongation of the Petit-Rhône canyon that seems to have been the main feeder throughout the Quaternary (Droz and Bellaiche, 1985). It represents an accumulation of ca. 3,600 m of turbidites and mass-transport deposits. On the the upper fan, between 1,350 m and 2,000 m water depths, a perched valley, 12 to 4 km wide and 500 to 200 m deep, is cut by a narrow, 1,000 to 600 m wide and 150 to 100 m deep, axial meandering channel (Lombo Tombo et al., 2015; O'Connell et al., 1991; Torres et al., 1997) (Fig. 1). The last channel avulsion most likely occurred during the LGM (Bonnel et al., 2005) and

led to the emplacement of a lobe-shaped fan, called neofan (Bonnel et al., 2005; Droz and Bellaiche, 1985; Jégou, 2008; Torres et al., 1997)}. (Fig. 1).

2.4 Slope instabilities

At the base of slope numerous headwall scars are indicative of slope failures (Berné et al., 2004; Droz and Bellaiche, 1985; Gaullier et al., 1998; Sultan et al., 2007; Torres et al., 1995). Scars are superimposed on a network of buried and active listric faults parallel to the margin (dos Reis et al., 2005; Torres et al., 1995) (Figs. 2). Although movements of these faults driven by halokinesis may be a pre-conditioning factor or even a trigger mechanism for sliding (Bellaiche et al., 1986; Droz, 1983) a causal link between these features has not yet been shown. Two large mass transport deposits are lying on the subsurface of the eastern and western sides of the fan and were named the Eastern and Western (superficial) Transparent Series (Bellaiche et al., 1986; Droz and Bellaiche, 1985), Intermediate Unit (Gaullier et al., 1998), Middle Unit (Méar and Gensous, 1993), Eastern and Western Debris Flow (Bonnel et al., 2005; Droz et al., 2001; Lastras et al., 2007a) and more recently Western and Eastern Mass Transport Deposits (WMTD and EMTD) (Droz et al., 2006). In this paper we will adopt the Rhone Western and Eastern Mass Transport Deposits (RWMTD and REMTD) nomenclature. These mass transport deposits are characterized by transparent seismic facies with no apparent internal structures apart from some undisturbed tilted block in the proximal area (Droz and Bellaiche, 1985). Concave and undulated features on top of both deposits, at the contact with adjacent undisturbed strata were interpreted as compression ridges formed by displaced material at the toe of the slope (Droz and Bellaiche, 1985). Scars surrounding both deposits are visible on the fan levees and on the adjacent base of slope suggesting that sliding has affected the whole base of slope and upfan area (Gaullier et al., 1998).

The age of these mass transport deposits remains speculative due to the lack of direct dating. Seismic stratigraphy and coring showed that both are covered by a metric pelagic drape and that the RWMTD is overlapped by the neofan deposits (Bonnel et al., 2005; Droz and Bellaiche, 1985; Gaullier et al., 1998; Torres et al., 1997; Torres et al., 1995) showing that turbiditic activity persisted after its emplacement, This suggests that both deposits probably emplaced during the Last Glacial Maximum, but close to the post-glacial sediment starvation of the Rhone fan dated at ca. 18.5 ka cal BP (Beaudouin et al., 2004; Dennielou et al., 2006; Lombo Tombo et al., 2015).

3. Data and methods

This study is based on a variety of bathymetry and seismic data collected since 1997 during several oceanographic campaigns (Fig. 3; Tab. 1) as well as on three piston cores (Tab. 2).

Two bathymetric Digital Terrain Models (DTMs) were used: a 500 m resolution DTM (IFREMER/CIESM, 2011) and unpublished 50 m and 100 m resolution DTMs based on Simrad EM12 and EM300 multibeam surveys during oceanic campaigns listed (Tab. 1).

Detailed mapping of the RWMTD is based on various seismic data including single and multi-channel GI and mini-GI (vertical resolution in the order of 30 and 10 m, respectively) High Resolution (HR) sparker lines as well as Very High Resolution (VHR) Sub-Bottom Profiler (SBP) lines (vertical resolution ca. 1 m) (Figs. 2, 3 and 4A; Tab. 1). This dense and multi-resolution seismic database allowed a detailed new mapping and characterization of the RWMTD and to produce isochore and isochron maps.

Two sediment cores were collected with the giant Calypso piston corer aboard R/V Marion Dufresne on the northern and southern extremities of the RWMTD. Another core was collected in the central part of the RWMTD with a Kullenberg piston corer aboard

R/V Le Suroit (Figs. 2, 3 and 4A; Tabs. 1 and 2). Identification of lithofacies and grain size is based on visual description and physical properties logging with a Geotek Multi-Sensor Core Logger. AMS radiocarbon dating was conducted on monospecific planktonic foraminifera (*Globigerina bulloides*). Age calibration into calendar scales was calculated by Calib 7.1 software (Stuiver et al., 2018) with the marine13 calibration curve (Reimer et al., 2013).

All data were integrated into the IHS Kingdom suite seismic interpretation software. For the interpolation of isochrone and isochore grid, we used the Flex Gridding algorithms, defining a cell size of 50 m. Conversion of seismic two-way travel times into meters in the sedimentary column was made with a sound velocity of 1600 $m.s^{-1}$, which may represent the minimum sound velocity according to wave velocities measured in sediment cores.

4. Results

4.1 Seabed morphology

The RWTMD has a faint expression on the seabed (Fig. 1) because it is partly overlain by more recent deposits that are the Rhone Neofan, the Pyreneo-Langudocian Sedimentary Ridge (Berné et al., 1999) and some deposits at the outlet of La Fonera canyon (Droz et al., 2001). The seabed morphology is also imprinted by erosional scours developed during the lowstand functioning of the Neofan (Bonnel et al., 2005) and of Cap de Creus canyon (Lastras et al., 2007b) which are still likely active due to deep water active hydro-sedimentary processes related to open-ocean convection (Stabholz et al., 2013).

The most obvious morphological evidence of mass wasting lies in the occurrence of slide scars in the proximal area of the RWMTD at the base of slope and on the side of the Rhone fan (Fig. 4B). All scars show a NE-SW orientation. The orientation of the biggest

scar, 30 km long, 10-100 m high headwall, running along slope and gradually becoming perpendicular to the slope on the side of Rhone fan between 2,000-1,900 m water depth, suggests a relation with the RWMTD (Fig. 4B). To the SW the headwall is nearly parallel to the slope at 2,100-2,200 m water depth, while to the NE it gradually becomes perpendicular to the slope between 2,000-1,900 m water depth, on the side of Rhone fan (Fig. 4B). Similar parallel headwalls, also facing to the SE, but shorter and discontinuous and less high are visible about 4 km upslope to the north (Fig. 4B). About 4 km to the south, on the side of the Rhone fan, a 15 km long headwall facing to the NW is perpendicular to the slope (Fig. 4B). The configuration of headwalls across the side of the Rhone fan forms a 7 km wide, 40 m deep along slope corridor that can be interpreted as a pathway for the RWMTD. Noteworthy, the scars are superimposed to the active and buried listric faults network developed by syn-sedimentary salt tectonics (dos Reis et al., 2005) (Fig. 4B).

To the south, the only obvious morphological expression of the RWMTD is a faint NE-SW lineation at the foot of a Rhone fan channel-levee and corresponding to a compression bulge at the lateral toe contact between the RWMTD and the Rhone fan (Fig. 4C).

4.2 Seismic structure of the RWMTD and of adjacent and underlying sediments

The RWMTD appears as a body with a transparent acoustic facies on the VHR, low penetration, SBP lines and on the HR single channel seismic lines (Figs. 5 to 9). However, on the 24-channel HR seismic it shows sub-continuous internal reflections roughly parallel to the seabed that onlap on the sedimentary basement (Fig. 5B). This is evidence that the infill occurred on an inherited morphology. In some areas the top reflector, close to the seabed, shows incisions and roughness, but in relation to more recent superficial deposits or hydro-sedimentary processes such as the neofan channels and

scours (Figs 6B, 7 and 8). Truncation of the Rhone fan strata (Fig. 5C) indicates that the RWMTD is related to the failure of the fan levee as also suggested by the collapsed western levee of the Rhone fan. (Fig. 4B).

The top of the RWMTD is rather smooth and shows a slope towards the SW and towards the south that roughly follows the overall trend of the underlying substratum (Fig. 10). To the north and to the south, the RWMTD outcrops, at least at the seismic vertical resolution, while in its central area it is overlapped to the east by the neofan deposits (Figs. 5D and 10A) and to the west by a thin veneer of Pyreneo-Langudocian Sedimentary Ridge deposits and of La Fonera canyon deposits (Fig. 5D, 7 and 8A). The compression bulge to the SE in the distal area is clearly visible and clearly shows that the RWMTD has overlapped the Rhone fan (Fig. 9).

On the VHR SBP lines the structure of the basement of the RWMTD is not visible because of the low seismic penetration. On VHR seismic, in the proximal (north) area the basement corresponds to stratified folded and/or faulted sediments characteristics of the base of slope deposits to the north (Fig. 5D) and Rhone fan stratified Pleistocene deposits to the east (Fig. 5). In the central area the RWMTD is confined between the Rhone fan deposits, to the east, where it pinches out, and the stratified deposits of the Pyreneo-Langudocian Sedimentary Ridge to the west (Figs. 6, 7, 8B and 9). From north to south the RWMTD width is ca. 40 km in the proximal area, 50 km in the central area and gradually narrows to 5 km in the most distal area. The horizontal run-out distance (L) is 180 km (Fig. 10), the height fall (H), i-e the height between the head scar and the most distal deposits is ca. 740 m and the H/L ratio is 0.004.

4.3 Extension, thickness and morphology at the base of the RWMTD

The RWMTD extends from 1,900 to 2,700 m water depth and covers a surface of 6800 km^2. The isochrones map of the basement shows that the RWMTD is emplaced in the large depression between the Rhone fan and the Catalan margin (Fig. 10B). The thickness of the RWMTD (Fig. 10C) is largely between 10 and 50 m thick, with the thickest deposits (67 m) located along a large valley against the Rhone fan (Fig. 10C). Otherwise, downslope, the thickness is rather constant and the volume of the RWMTD is estimated at 160 km^3. By comparison earlier mapping with low resolution seismic gave a surface of ca. 7500 km^2 with a thickness up to 120 mstwtt (96 m) and commonly around 50 mstwtt (40 m) for an estimated volume of 230 km^3 (calculation after Gaullier et al. (1998) with the same velocities as this study). For further comparison, the REMTD covers an area of 7800 km^2 with a thickness up to 160 mstwtt (128 m) and commonly around 50-100 mstwtt (40-80 m) for an estimated volume of 170 km^3 (Coutellier, 1985; Droz and Bellaiche, 1985)

The morphology at the base of the RWMTD is very different from the present-day seabed. Besides an overall slope gradient to the SW and south, it shows a complex morphology characterized by highs and lows. To the north the most proximal deposits lie on stair-like morphologies corresponding to the tip of listric faults (Fig. 5D). To the east, the contact with the adjacent Rhone fan is characterized by truncations of the fan levees indicative of failure and collapse of the levee (Fig. 5C). To the south the RWMTD fills several depressions that build a 12 to 18 km wide and 30 m deep valley against the Rhone fan (Figs 5C, 7 and 9) in the continuation of the present Sète canyon outlet, widening downslope and that connects to the Valencia valley. The RWMTD shows a bifurcation to the SW where it becomes narrower (5 km) and connects to the Clots del Puget and Valencia valleys (Figs. 8C and 8D). A parallel but fainter valley also runs along the Pyreneo-Langudocian Sedimentary Ridge (Fig. 10B). This buried valley to the east

shows a concave-up longitudinal profile that fits with the concave-up longitudinal shape of the Sète canyon and Valencia channel suggesting that the three valleys were a continuum before the emplacement of the RWMTD (Fig. 10D).

4.4 Lithofacies and chronology of the RWMTD

Three sediment cores were collected in areas where the RWMTD outcrops at the seabed at the seismic resolution. Core MD01-2435 was collected at a RWMTD proximal location where the WMTD lies on the Rhone fan deposits (Fig. 6A), core KSGC-10 was collected at a RWMTD central location on the neofan area where scours have eroded into the RWMTD and open-ocean convection has prevented the deposition of sediment since beginning of the Holocene (Dennielou et al., 2009; Stabholz et al., 2013), core MD01-2438 was collected at a RWMTD distal location (Figs. 2, 3 and 6B). Sediment in MD01 cores show disturbance related to non-stationary behaviour of the piston, which led to oversampling during coring (Bourillet et al., 2007; Skinner and McCave, 2003), thus preventing straightforward correlation between cores and seismic data. However, the identification of lithofacies was still possible, and sharp contrasts between pelagic, turbiditic and mass transport deposits make straightforward the analogy between lithofacies and well-contrasted seismic facies.

Three sedimentary units were identified (Fig. 11). Unit 1 is composed of foraminifera and calcareous nannoplankton oozes that correspond to ambient pelagic sedimentation. Unit 2 is composed of laminated mud with frequent silt to very fine sand laminae. This facies is interpreted as turbidites deposited by turbidity current spillover from the adjacent perched valley. They are similar to those already described in the Rhone fan valley or on the neofan levees (Bonnel et al., 2005; Dennielou et al., 2006; Lombo Tombo et al., 2015). Unit 3 is composed of stiff mud with colour banding corresponding to

sulphide rich laminae and few silt layers characteristics of lithofacies in the Rhone fan (Lombo Tombo et al., 2015). Laminae are either horizontal, oblique or show tight folding. In core MD01-2438 a layer of coarse material in the form of fine to very coarse sand bioclasts and lithoclasts have been involved in the sediment deformation but no evidence of matrix supported clasts or blocks was found. This lithofacies is much denser (>2 $g.cm^{-3}$) and stiffer than the units above with similar (muddy) grain sizes (Fig. 11) suggesting that it is over-consolidated and was therefore either previously buried deeper than its present stratigraphic depth or has gained strength after remoulding. The unit is interpreted as the RWMTD deposits. The plastic deformation and contortion are indicative of shearing and the lack of faulting and blocks show that the sediment remained a coherent mass, at least for the upper sampled part, so that the RWMTD can be classified as a slide or slump because of evidence of plastic deformation (cf. Mulder and Cochonat (1996); Piper et al. (1997); Tripsanas et al. (2008); Nelson et al. (2011); Shanmugam (2015)). The transparent echo-facies that characterizes the RWMTD is commonly interpreted as indicative of disintegration as a result of break up of blocks in the downslope evolution of a slide into a debris flow (Piper et al. 1997). The absence of blocks in the retrieved sediment cores may be due to the low penetration. However, the sediment contortion is also a factor of strata disorganisation consistent with the transparent echo-facies.

In core MD01-2435 (Fig. 11) Unit 1 is described from top to 0.25 m and Unit 2 from 0.25 to 8.90 m. The contact between the units is oblique and erosional. Unit 3 is described from 8.90 to 15,50 m, colour banding is horizontal to sub-horizontal (up to 15° inclination) but inclination varies down core. From 15.50 m to the base of core, the sediment is fully disturbed because it was sucked up during coring, however, despite disturbance the collected sediment is very similar to Unit 3.

In core KSGC-10 (Fig. 11), only Unit 3 is present showing that no sediments were deposited during the Holocene (Dennielou et al., 2009; Stabholz et al., 2013).

In core MD01-2438 (Fig. 11) Unit 1 is described from 0 to 1.00 m. Two layers of coarse sand (2 and 16 cm thick) are intercalated in the unit and correspond to post-glacial and Holocene turbidites already described at the base of slope of the study area (Dennielou et al., 2009). Unit 2 is not present and Unit 1 rests on Unit 3. Unit 3 is described from 1.00 m to the base of core (8.00 m), the contact between Unit 1 and 3 is sharp and horizontal. Colour banding is contorted from 1.00 m to 5.00 m and becomes gradually horizontal to sub-horizontal downcore. From 8.00 m to the base of core the sediment is also fully disturbed and the collected sediment is very similar to Unit 3.

Radiocarbon dating (Tab. 3 and Fig. 11) shows that the hemipelagic Unit 1 was deposited during the deglacial sea level rise and during the Holocene highstand and that turbiditic Unit 2 was deposited at the end of the LGM during and shortly after the onset of the sea level rise (20.7-14.7 ka cal BP). These ages are consistent with those obtained for the same units on the Rhone fan and adjacent areas (Beaudouin et al., 2004; Bonnel et al., 2005; Dennielou et al., 2006; Dennielou et al., 2009; Lombo Tombo et al., 2015). Ages obtained at the top of the RWMTD (Unit 3) and at the base of overlapping units (turbiditic Unit 2 in the proximal position and Unit 1 in the distal position) are similar and show that emplacement of the RWMTD occurred between 19.9 and 21.5 ka cal BP (2 sigma) with an average median age of 21.0 ka cal BP (Fig. 12). However, this does not discard a possibility of several stages of sliding in this age bracket.

5. Discussion

5.1. The Rhone WMTD: a hidden landslide

Unlike several recent mass transport deposits around the world (e.g. Storegga (Bugge et al., 1988), BIG'95 (Lastras et al., 2002), Ruatoria (Collot et al., 2001), among the largest), the RWMTD has a faint seabed morphological expression and could be easily overlooked if no seismic data was available. The lack of morphologic expression is a consequence of two factors : (1) the fact that displaced and deposited sediment infilled the topographic low between the Rhone fan and Pyreneo-Languedocian Sedimentary Ridge and adjacent slope to the west (Fig. 1) and did not created any distal positive relief, (2) seabed rejuvenation by rapid burying related the high sedimentation rates that persisted at the base of slope until 18.5 ka BP (Bonnel et al., 2005; Lombo Tombo et al., 2015), i-e during ca. 1.5 to 3.5 ka after the emplacement of the RWMTDT, and by the development of the neofan avulsion lobe and channel-levee on top of it.

At river mouth subaqueous deltas or upper slopes under high sedimentation rates sliding seems to be a frequent quasi intrinsic process of sediment movement and transfer but resulting morphologies are quickly buried and obscured, sometimes within days to years (Biscara et al., 2012; Clare et al., 2016 ; Kelner et al., 2014; Mazières et al., 2014; Obelcz et al., 2017; Smith et al., 2007). Our study shows that obscuration may occur on much larger areas at slope bases. Indeed, the RWMTD case may be atypical but it raises the question of the recognition of large mass transport deposits and outlines that bathymetric data alone are not sufficient for their recognition on high sedimentation rate continental margins such as glacigenic and deltaic margins and that inventories (e.g. Urgeles and Camerlenghi, (2013)) may be incomplete at the largest end of the spectrum.

5.2. Source and trigger mechanisms

The recurrence of mass transport deposits in many deep-sea fans on deltaic margins such as the Mississippi (Twichell et al., 1991; Weimer, 1989), Amazon (Piper et al., 1997), Danube (Popescu et al., 2001) or Nile (Garziglia et al., 2008) shows that sediment loading, mostly during lowstands, is a major preconditioning factor for sliding. Sliding can occur when the stress exceeds the sediment strength and no external trigger mechanism is actually needed to explain sliding of high sedimentation rate poorly-consolidated sediment, even with low slopes, (Croguennec et al., 2017; Dennielou et al., 2017). This configuration can be clearly invoked for the Rhone slope and fan where high sedimentation rates, in the order of several meters per thousand years, during the Last Glacial Maximum (Lombo Tombo et al., 2015; Sierro et al., 2009) have shortly preceded the emplacement of the RWMTD. Among preconditioning factors, the occurrence of a presently buried valley adjacent to the Rhone fan, in the continuation of the Sète valley, suggests oversteepening by lateral retrogressive erosion along the Rhone fan. This process has been proposed for explaining the broadening of the Bourcart Canyon (Baztan et al., 2005; Sultan et al., 2007). At some stage, these recurrent failures may have triggered a massive retrogressive failure of the fan levee and adjacent slope. Another preconditioning factor could be local slope oversteepening by vertical movements of listric faults (dos Reis et al., 2005) (Fig. 4B).

External triggers can occur and hasten sliding. In the GoL. earthquake shaking can be discarded as the GoL is a low seismicity area where during the last 50 years most earthquake magnitudes were lower than 4 (Manchuel et al., 2017). Furthermore, a minimum magnitude of 7 is needed to trigger instabilities on high sedimentation rate lowstand sediments in the neighbouring Bourcart Canyon (Sultan et al., 2007).

5.3. Processes for propagation and long runout distance

The RWMTD appears as a seismically homogenous and transparent body with no evidence of particular internal structure. A large part of the body is buried under late and post-glacial turbiditic deposits and erosions that might have obliterated morphological features on top of the RWMTD (Bonnel et al., 2005; Droz and Bellaiche, 1985; Gaullier et al., 1998; Torres et al., 1997). However, seismic data reveal a rather flat morphology on top (Figs. 6 to 10) and do not show evidence of faulting, blocks formation, rafting or retrogression as observed in the neighbouring Big'95 landslide on the Ebro Margin (Lastras et al., 2002; Lastras et al., 2004). On the contrary, the RWMTD shows evidence of widespread ductile-plastic behaviour with folding and contortion in the clay-rich sampled sediment (Fig. 11), and the formation of a compression bulge at the SE limit against the Rhone fan (Figs. 4C, 4D and 9). The ductile-plastic interpretation is reinforced by the fact that the RWMTD has spread onto and filled the pre-existing seabed morphologies (Figs. 5 to 10).

Mass transport deposits can propagate over very long distances, in the order of several hundreds of kilometres for the largests, and the runout distance is roughly proportional to the size of the slide (De Blasio and Elverhøi, 2011; Haflidason et al., 2005). The RWMTD exhibits a H/L ratio in the order of 0.004, which fits within the morphometric characteristics of many mass transport deposits in the world (Issler et al., 2005). In particular, it fits particularly well with the characteristics of the Storegga's 63 slide lobes (Haflidason et al., 2005; Issler et al., 2005) suggesting that they share common mechanical properties and propagation processes. Indeed, like the Storrega slide, the RWMTD involved clay-rich sediments but with drastically different sources because the Norwegian margin is fed by glacial and glacigenic sediments, while the GoL is fed by temperate deltaic sediments. Many studies outline a discrepancy between the mechanical properties (high strength, high density, low porosity) of cohesive sediment

448 in mass transport deposits and their exceptional long runout distances that would
449 necessitate much lower sediment strength (De Blasio et al., 2005). This is also the case
450 for the RWMTD that exhibits clay-rich sediments with exceptional high densities
451 (between 2 and 2.2 $g.cm^{-3}$) that evidence over-consolidation with regards to the
452 overlying sediment (Fig. 11). Modelling of long runout distance by viscoplastic model
453 requires to introduce very low sediment strength (De Blasio et al., 2005), much lower
454 than that of the slided sediment and of the mass transport deposit. However,
455 remoulding of sediment and adjunction of water (shear wetting) during transport can
456 significantly decrease the sediment strength (De Blasio et al., 2005) and enhance
457 lubrication at the base and front of the mass transport deposit and explain long runout
458 distances (De Blasio and Elverhøi, 2011). In addition, hydroplaning may also increase
459 lubrication (De Blasio et al., 2005; Mohrig et al., 1998). The present high density of the
460 RWMTD suggests a drastic strengthening of sediment during transport or after
461 transport. Sediment densification is a common feature of mass transport deposits that
462 occurs in response of shearing in highly sensitive clays and explaining that they exhibit
463 contrasted impedance with the surrounding sediment and are very well imaged on
464 seismic data (Dugan, 2012). The important folding and contortion in the clay sediment
465 sampled on the top 7 m of the RWMTD at proximal, central and distal locations, is an
466 evidence that shearing occurred during transport and may thus explain the present high
467 density.
468
469 **5.4. Timing and synchronism with other major sediment gravity deposits in the**
470 **north-western Mediterranean**
471 The emplacement of the RWMTD is dated during the LGM between 19.9-21.5 ka cal BP
472 (end of the LGM) according to our radiocarbon dating at the base of sediment drape on

473 top of the RWMTD (Fig. 11). In the north-western Mediterranean, this period of time and
474 the ensuing post-glacial sea level rise are characterized by several other major events
475 that are the BIG'95 mass transport deposit (26 km^3) on the Catalan-Ebro margin
476 (Lastras et al. 2002), the Rhone EMTD (150-200 km^3) (Droz and Bellaiche, 1985; Droz et
477 al. 2006) in the GoL, and the megaturbidite in the Balearic Abyssal Plain (ca. 500 km^3)
478 (Rothwell et al., 1998).
479 The BIG'95, seems to have been emplaced in a different setting than that of the RWMTD.
480 It affected the Ebro fed clay-rich deposits but that, unlike the Rhone fed deposits, are
481 less focused and spread through several canyons and developed at the base-of-slope
482 several channel–levee complexes with an apron-ramp turbidite system (Alonso and
483 Maldonado, 1990; Lastras et al., 2004). Sliding and long runout occurred at shallower
484 water depth from the upper slope at 200 m water depth to 2000 m water depth (and
485 more recently, at the end of the deglacial sea level rise at 11.0-11.5 ka cal BP (Lastras et
486 al., 2002; Lastras et al., 2004). However, like for the RWMTD, high sediment load and
487 over-steepening during lowstand may have been a determinant trigger mechanism
488 (Lastras et al., 2004).
489 The age of the REMTD is still unknown but like the RWMTD it is very shallow, it also
490 involved adjacent turbidite leveed deposits and it lies at the same water depths (1,900-
491 2,700 m). Although both deposits are clearly separated by the Rhone deep-sea turbiditic
492 valley (Droz and Bellaiche, 1985), it is quite likely that their emplacement is coeval,
493 share common trigger mechanisms and that may even correspond to a single event.
494 Megaturbidites are interpreted as the possible product of massive slope failures that
495 evolved into turbidity current(s) eventually deposited and trapped in the deepest part of
496 closed oceanic basins like in the Mediterranean (Cita and Aloisi, 2000; Reeder et al.,
497 2000). Exceptional high-impact hazards capable of broadly shaking or reworking

sediments on slopes such as volcanic eruptions, earthquakes and tsunamis have been suggested as a trigger mechanism (San Pedro et al., 2017), but environment-climatic driven triggers such as sea-level change or gas hydrate destabilisation are also evoked (Reeder et al., 2000; Rothwell et al., 2000). A 8–10 m thick dominantly muddy megaturbidite fills the whole Balearic Abyssal Plain over 60,000 km^2. In seismic data it appears as a laterally continuous, acoustically transparent layer (Rothwell et al., 1998). The source remains unknown but thickening and coarsening of the basal sand of the megabed towards the north suggests emplacement from that direction (Rothwell et al., 1998). The calibration of the weighted mean radiocarbon age obtained on top of the megabed by Rothwell et al. (1998) gives a 2 sigma age comprised between 20.3 and 20.9 ka cal BP with a median probability of 20.6 ka cal BP (Reimer et al., 2013) but the group of dates obtained is bracketed between 19.5 and 21.7 ka cal BP (Fig. 12). Therefore, ages of both RWMTD and Balearic Abyssal Plain megaturbidite are the same within 2-sigma confidence interval and no chronological order can be given between the two deposits, reinforcing the possibility of a genetic link compatible with the proposed northern source. However, the exceptional volume of the Balearic Abyssal Plain megaturbidite shows that the related mass movement was likely efficiently evacuated from the source failure, which is not the case of the RWMTD and REMTD. Therefore, even though the RWMTD and REMTD may have contributed to feed the megaturbidite, the failure source must be also sought in adjacent areas characterized by recurrent slope failures like the Ligurian margin (Ioualalen et al., 2010; Migeon et al., 2011).

5.5. Consequences on sediment routing in the western Gulf of Lions rise and Rhone fan

Sedimentation and sediment transfer processes in the GoL and Catalan-Ebro margins are characterized by high sediment input from the Rhone and Ebro River and by numerous canyons dissecting the outer shelf and slope efficiently draining sediments towards the base of slope. The transfer was obviously efficient during the LGM lowstand with the growth of the deep-sea fans and sedimentary ridges (Beaudouin et al., 2004; Jallet and Giresse, 2005; Lombo Tombo et al., 2015; Melki et al., 2009). Even during the Holocene highstand, although sediment fluxes at the shelf break are several orders of magnitude lower than during the LGM, canyons remain an efficient pathway as they can focus high amplitude hydro-sedimentary processes with a strong imprint on the sea bed morphology (Canals et al., 2006; Lastras et al., 2007b; Palanques et al., 2006; Payo-Payo et al., 2017) and even deposit sandy turbidites at the base of slope (Dennielou et al., 2009). In the western part of the GoL, the Sète canyon network, the La Fonera canyon and the Clots del Puget canyon presently reach the base of slope and vanish at ca. 2300 m (Fig. 1).

The longitudinal concave-up shape of the buried valley along the western flank of the Rhone fan, in the direct prolongation and in good fit with the concave-up longitudinal shape of the Sète canyon and the Valencia channel (Figs. 10B, C, D and 13A), shows that during the LGM, prior to the emplacement of the RWMTD, the western GoL canyon drainage network and the Ebro-Valence canyon drainage networks were coalescing and that, probably, the Valencia fan was collecting significantly more important volumes of sediment (Fig. 13A). The presence of such an important erosional channel questions about the sediment source and flow capable of developing and maintaining this conduit. The presence of an axial incision in several canyons (Bourcart, Herault and Marti) suggests that these canyons heads were connected with major rivers during the last glaciation and were fed by sustained confined turbidity currents (Baztan et al., 2005).

This is confirmed by the mapping of the LGM paleo-fluvial drainage network on the shelf that shows that the Herault canyon was fed by the Rhone River (Jouet et al., 2006) and may have supplied frequent turbiditic flows to develop the valley.

The burying and clogging of this channel resulted in a major reorganisation of the sediment routing in the north-western Mediterranean. It is not possible to determine the magnitude of the decrease in the quantity of sediment supply into the Valencia channel, but this question could be easily addressed by collecting sediments cores along the Valencia channel, both upstream and downstream of the channels coalescence. The RWMTD was not found inside the Valencia valley, while it is still visible inside the extremity of the Clots del Puget/Entrant de Palamos valley where both valleys coalesced (Fig. 8D). Indeed, the RWMTD may have never been engaged inside the Valencia channel, but it is also possible that deposits have been eroded and removed from the valley. This is also suggested by evidences of upstream erosion in the Valencia channel, in the order of several meters per thousand years since the LGM (Amblas et al., 2011).

A close examination of seabed morphology at the outlet of the Sète canyon network shows large erosive bedforms in the distal reaches, including grooves and crescent scours (Lastras et al., 2007b) and shows that the seabed has a concave-up shape on top of the RWMTD (Fig. 4B and 4D). This is indicative that bed-load sediment transport with dominantly bypassing and erosive processes have persisted down the Sète canyon network during the LGM after the emplacement of the RWMTD and have started the excavation of a new drainage at the same location of the buried one. Shallow, lobe-shaped deposits, such as the Sète lobe (Droz et al., 2001), at the extremity of the canyon are also suspected (Fig. 13B). There are also evidences of currently active hydro-sedimentary processes in the Cap de Creus canyon such as dense water cascading

capable of transporting huge quantities of sediment (Canals et al., 2006; Lastras et al., 2007b; Palanques et al., 2009) further suggesting that excavation is still ongoing.

We have shown that several sediment failures that fed the RWMTD have affected the Rhone fan deposits and that headscars have even nearly reached the perched valley (Fig. 4B and 6A). The last, westward, avulsion of the Rhone deep-sea channel occurred shortly after the emplacement of the RWMTD as indicated by the subsequently deposited neofan resting on top of the RWMTD (Figs. 5 to 8) (Droz and Bellaiche, 1985; Torres et al., 1997). Interestingly, the channel avulsion occurred in an area where the RWMTD extends onto the Rhone levee and that can be interpreted as a failure area similar to that further north (Fig. 4B and 5C). Therefore one can argue that channel avulsion may have been triggered after breaching of the levee by the failure of the levee, although downstream clogging of the Rhone channel is also evoked (Droz and Bellaiche, 1985).

The major disruptions in the sediment routing occurred shortly (ca. 3 ky) before the onset of the post-glacial sea level rise at ca. 18.5 cal. ka BP and the sediment starvation of slope and base-of-slope fans consecutive to the backstepping of sediment depocenters onto the shelf (Berné et al., 2007; Lombo Tombo et al., 2015). Therefore the consequences on the sedimentation in the Valencia fan, the final sink, may not be well visible and recorded. It is possible to extrapolate the consequences during a future lowstand. Since there are evidences that the concave-up morphology at the base of slope has already started to recover, one can argue that during a future lowstand the recovery may be complete and that the Valencia channel may collect again the sediments from the Sète canyon network, but, in addition and this is a major contrast with the LGM, the neochannel avulsion will possibly also route the Rhone sediment into the Valencia channel and fan making it the collector from the two major north-western

596 Mediterranean rivers, the Ebro and the Rhone. However, this would be a temporary
597 situation because the Rhone levees display several collapses prone to trigger breaches
598 and new channel avulsions (Fig. 4B and 6A).
599
600 **5.6. Significance for sediment routing in the submarine realm**
601 Modification of sediment transport pathways in the terrestrial realm by rerouting of
602 rivers after hillslope landslides or glacier retreat is well documented and major (>10^5
603 m^3) terrestrial landslides can instantaneously modify river pathways for periods of
604 times relevant to landscape evolution (>10^4 yr) (Ouimet et al., 2007; Shugar et al., 2017).
605 Large landslides can also act as a primary control on channel morphology and
606 longitudinal river profiles, modify the adjustment of rivers to regional tectonic, climatic,
607 and lithologic forcing (Ouimet et al., 2007), and therefore influence the volume and rates
608 of sediment delivered into the oceans. Though marine landslide volumes are up to three
609 order of magnitude larger than their aerial counterparts (Hampton et al., 1996; Urgeles
610 and Camerlenghi, 2013) and are major elements of sedimentary margin development,
611 their contribution to deep-sea sediment routing is not well documented. As a
612 consequence of their widespread occurrence in turbidite systems, landslides, mass
613 transport deposits or mass transport complexes play a significant role in the topography
614 of channels or slopes, affect the resulting accommodation space, the development and
615 bifurcation of deep-sea channel, and *in fine* can control the routing and dispersal of
616 sediment at the fan scale (Armitage et al., 2009; Bernhardt et al., 2012; Corella et al.,
617 2016; Kawamura et al., 2010; Kneller et al., 2016; Ortiz-Karpf et al., 2015). However, a
618 fundamental modification of a deep-sea sediment transport network by a single
619 submarine mass transport deposit at continental margin scale seems unprecedented.
620 Noteworthy, the present case also involves rapid turbidite accumulation showing that

rapid changes of sediment routing may occur in areas of massive sediment deposition prone to rapid evolution of submarine morphologies. We suggest that the converging pattern of the canyon network as well as the semi-confined morphology at the base of slope of the western part of the GoL created a receptacle suitable for rapid infill and blocking of canyons.

6. Conclusions

A comprehensive mapping of the Rhone RWMTD was performed, based on seismic data collected during several oceanographic campaigns between 1997 and 2008. The RWMTD emplaced on the western flank of the Rhone fan and involved sediment from the base of slope and from the adjacent Rhone fan levee. The RWMTD covers a surface of 6800 km^2. It represents a volume of 160 km^3 of folded and contorted laminated clayey high-density stiff sediments that have spread over 180 km.

Our results show that :

- Large mass transport deposits can be obscured in settings where sedimentation rates are high. This underlines the importance of integrated (swath bathymetric, seismics, core data) studies, and also suggests that hazard catalogues constructed from seafloor morphology alone may be incomplete.
- Mass wasting is a major process of the margin development in the GoL and more generally in the north-western Mediterranean. Several very large events occurred within a very small time window in the Western Mediterranean (Rhone Western and Eastern mass transport deposits and Balearic Abyssal Plain megaturbidite) and account for a significant proportion of the stratigraphy. Though probably not genetically linked, they occurred in period of time of large sediment transport into the base of slope during the Last Glacial Maximum.

- Large landslide deposits can fundamentally modify sediment routing systems in the marine realm at margin scale. Mass wasting must therefore be considered as a major internal forcing on sediment dispersal. These drastic events can have a major impact on downstream sedimentation at the base of slope and abyssal plains where sedimentation is therefore not only controlled by externally forced fluctuations of sea level and sediment flux.

It can be pointed out that the emplacement of the RWMTD in the lowstand systems tract, shortly (1-2 ky) before the onset of the post-glacial sea level rise and Rhone fan sediment starvation (Lombo Tombo et al., 2015), is conform to the Exxon sequence stratigraphy sea-level based model.

Acknowledgements

We thank chief scientists, shipboard scientific parties, captains and crews of oceanographic campaigns that allowed collection of the data used in this paper. IFREMER's technical staff from sediment analysis platform (René Kerbrat, Gilbert Floch, Mickael Rovere, Angélique Roubi) and from Service Cartographie, Traitement de Données et Instrumentation (CTDI) is thank for its help. I.J. was supported by a post-doc grant from Institut Carnot IFREMER EDROME, a program from ANR (Agence Nationale de la Recherche). This work was supported by the European Training Network SLATE (Submarine Landslides and their impact on European continental margins) within the Framework Programme for Research and Innovation Horizon 2020 under Grant Agreement No 721403. We thank Jason D. Chaytor and Mike A. Clare for their substantial and constructive reviews and guest editor Veerle Huvenne for the careful final reading that greatly improved the manuscript. This paper is dedicated to Jean-Pierre Henriet who was the head of IFREMER's "Département Géosciences Marines"

671 between 1990 and 1995. As a Director, Jean-Pierre had a strong imprint on the
672 development of studies on sedimentary environments within the Geosciences
673 Department of IFREMER.
674
675 **Sample list**
676 Core MD01-2435: http://igsn.org/BFBGX-88347
677 Core KSGC-10: http://igsn.org/BFBGX-87938
678 Core MD01-2438: http://igsn.org/BFBGX-88349
679
680 **References**
681 Alonso, B. and Maldonado, A., 1990. Late Quaternary sedimentation patterns of the Ebro
682 turbidite systems (northwestern Mediterranean): Two styles of deep-sea
683 deposition. Marine Geology, 95(3): 353-377. https://doi.org/10.1016/0025-
684 3227(90)90124-3
685 Amblas, D., Canals, M., Urgeles, R., Lastras, G., Liquete, C., Hughes-Clarke, J.E., Casamor,
686 J.L. and Calafat, A.M., 2006. Morphogenetic mesoscale analysis of the
687 northeastern Iberian margin, NW Mediterranean Basin. Marine Geology, 234(1-
688 4): 3-20. https://doi.org/10.1016/j.margeo.2006.09.009
689 Amblas, D., Gerber, T.P., Canals, M., Pratson, L.F., Urgeles, R., Lastras, G. and Calafat, A.M.,
690 2011. Transient erosion in the Valencia Trough turbidite systems, NW
691 Mediterranean Basin. Geomorphology, 130(3-4): 173-184.
692 http://dx.doi.org/10.1016/j.geomorph.2011.03.013
693 Armitage, D.A., Romans, B.W., Covault, J.A. and Graham, S.A., 2009. The Influence of
694 Mass-Transport-Deposit Surface Topography on the Evolution of Turbidite
695 Architecture: The Sierra Contreras, Tres Pasos Formation (Cretaceous), Southern

696 Chile. Journal of Sédimentary Research, 79(5): 287-301.
697 https://doi.org/10.2110/jsr.2009.035
698 Aslanian, D., Géli, L. and Olivet, J.-L., 2006. SARDINIA cruise, RV L'Atalante.
699 http://dx.doi.org/10.17600/6010150
700 Bassetti, M.A., Berné, S., Jouet, G., Taviani, M., Dennielou, B., Flores, J.-A., Gaillot, A.,
701 Gelfort, R., Lafuerza, S. and Sultan, N., 2008. 100-ka and rapid sea-level changes
702 recorded by prograding shelf sand bodies in the Gulf of Lions (Western
703 Mediterranean). Geochemistry, Geophysics, and Geosystems, 9(11): Q11R05.
704 https://doi.org/doi:10.1029/2007GC001854
705 Baztan, J., Berné, S., Olivet, J.-L., Rabineau, M., Aslanian, D., Gaudin, M., Réhault, J.-P. and
706 Canals, M., 2005. Axial incision, the key to understand submarine canyon
707 evolution (in the western gulf of Lion). Marine and Petroleum Geology, 22(6-7):
708 805-806. https://doi.org/10.1016/j.marpetgeo.2005.03.011
709 Beaudouin, C., Dennielou, B., Melki, T., Guichard, F., Kallel, N., Berne, S. and Huchon, A.,
710 2004. The Late-Quaternary climatic signal recorded in a deep-sea turbiditic levee
711 (Rhone Neofan, Gulf of Lions, NW Mediterranean): palynological constraints.
712 Sedimentary Geology, 172(1-2): 85-97.
713 https://doi.org/10.1016/j.sedgeo.2004.07.008
714 Bellaiche, G., Coutellier, V. and Droz, L., 1986. Seismic evidence of widespread mass
715 transport deposits in the Rhône deep-sea fan: Their role in the fan construction.
716 Marine Geology, 71(3): 327-340. https://doi.org/10.1016/0025-
717 3227(86)90076-9
718 Berné, S., 2000. MARION cruise, RV Le Suroît. http://dx.doi.org/10.17600/20110
719 Berné, S. and Dennielou, B., 2008. RHOSOS cruise, RV Le Suroît.
720 http://dx.doi.org/10.17600/8020040

721 Berné, S., Jouet, G., Bassetti, M.A., Dennielou, B. and Taviani, M., 2007. Late Glacial to
722 Preboreal sea-level rise recorded by the Rhone deltaic system (NW
723 Mediterranean). Marine Geology, 245(1-4): 65-88.
724 https://doi.org/10.1016/j.margeo.2007.07.006
725 Berné, S., Loubrieu, B. and embarquée, l.E.C., 1999. Canyons et processus sédimentaires
726 récents sur la marge occidentale du Golfe du Lion. Premiers résultats de la
727 campagne Calmar. Comptes Rendus de l'Académie des Sciences - Series IIA -
728 Earth and Planetary Science, 328(7): 471-477. https://doi.org/10.1016/S1251-
729 8050(99)80148-7
730 Berné, S., Satra, C., Aloïsi, J.-C., Baztan, J., Dennielou, B., Droz, L., Dos Reis, A.T., Lofi, J.,
731 Méar, Y. and Marina, R., 2004. Carte morpho-bathymétrique du Golfe du Lion,
732 notice explicative. Ifremer, QUAE, http://www.quae.com/fr/r411-le-golfe-du-
733 lion-carte-morpho-bathymetrique.html
734 Bernhardt, A., Stright, L. and Lowe, D.R., 2012. Channelized debris-flow deposits and
735 their impact on turbidity currents: The Puchkirchen axial channel belt in the
736 Austrian Molasse Basin. Sedimentology, 59(7): 2042-2070.
737 https://doi.org/10.1111/j.1365-3091.2012.01334.x
738 Biscara, L., Hanquiez, V., Leynaud, D., Marieu, V., Mulder, T., Gallissaires, J.M., Crespin, J.P.,
739 Braccini, E. and Garlan, T., 2012. Submarine slide initiation and evolution
740 offshore Pointe Odden, Gabon ,Äî Analysis from annual bathymetric data
741 (2004,Äì2009). Marine Geology, 299-302: 43-50.
742 https://doi.org/10.1016/j.margeo.2011.11.008
743 Bonnel, C., Dennielou, B., Berné, S., Mulder, T. and Droz, L., 2005. Architecture and
744 depositional pattern of the Rhône Neofan and recent gravity activity in the Gulf of

745 Lions (Western Mediterranean). Marine and Petroleum Geology, 22(6-7): 827-
746 843. https://doi.org/10.1016/j.marpetgeo.2005.03.003
747 Bourcart, J., 1960. Carte topographique du fond de la Méditerrannée Occidentale.
748 Bulletin de l'Institut Océanographique, 1163: 1-20.
749 Bourillet, J.-F., Damy, G., Dussud, L., Sultan, N., Woerther, P. and Migeon, S., 2007.
750 Behaviour of a piston corer from accelerometers and new insights on quality of
751 the recovery, Proceedings of the 6th International Off shore Site Investigation
752 and Geotechnics Conference: Confronting New Challenges and Sharing
753 Knowledge, 11-13 September 2007, London, UK, pp. 57-62.
754 Bryn, P., Berg, K., Forsberg, C.F., Solheim, A. and Kvalstad, T.J., 2005. Explaining the
755 Storegga Slide. Marine and Petroleum Geology, 22(1): 11-19.
756 https://doi.org/10.1016/j.marpetgeo.2004.12.003
757 Bugge, T., Belderson, R. and Kenyon, N.H., 1988. The Storegga slide. Philosophical
758 Transactions of the Royal Society of London. Series A, Mathematical and Physical
759 Sciences, 325(1586): 357. https://doi.org/10.1098/rsta.1988.0055
760 Canals, M., Puig, P., Durrieu de Madron, X., Heussner, S., Palanques, A. and Fabres, J.,
761 2006. Flushing submarine canyons. Nature, 444(7117): 354-355.
762 https://doi.org/10.1038/nature05271
763 Canals, M., Serra, J. and Riba, O., 1983. Toponímia de la Mar Catalano-Balear. Bol. Soc.
764 Hist. Nat Baleares, 1982(2): 48-58.
765 http://www.raco.cat/index.php/BolletiSHNBalears/article/download/171046/
766 244849
767 Cita, M.B. and Aloisi, G., 2000. Deep-sea tsunami deposits triggered by the explosion of
768 Santorini (3500y BP), eastern Mediterranean. Sedimentary Geology, 135(1): 181-
769 203. https://doi.org/10.1016/S0037-0738(00)00071-3

770 Clare, M.A., Hughes Clarke, J.E., Talling, P.J., Cartigny, M.J.B. and Pratomo, D.G., 2016.
771 Preconditioning and triggering of offshore slope failures and turbidity currents
772 revealed by most detailed monitoring yet at a fjord-head delta. Earth and
773 planetary science letters, 450: 208-220.
774 https://doi.org/10.1016/j.epsl.2016.06.021
775 Clark, P.U., Archer, D., Pollard, D., Blum, J.D., Rial, J.A., Brovkin, V., Mix, A.C., Pisias, N.G.
776 and Roy, M., 2006. The middle Pleistocene transition: characteristics,
777 mechanisms, and implications for long-term changes in atmospheric pCO2.
778 Quaternary Science Reviews, 25(23): 3150-3184.
779 https://doi.org/10.1016/j.quascirev.2006.07.008
780 Cochonat, P., 2001. GMO1 cruise, RV Le Suroît. http://dx.doi.org/10.17600/1020040
781 Collot, J.-Y., Lewis, K., Lamarche, G. and Lallemand, S., 2001. The giant Ruatoria debris
782 avalanche on the northern Hikurangi margin, New Zealand: Result of oblique
783 seamount subduction. Journal of Geophysical Research: Solid Earth, 106(B9):
784 19271-19297. https://doi.org/10.1029/2001JB900004
785 Corella, J.P., Loizeau, J.L., Kremer, K., Hilbe, M., Gerard, J., le Dantec, N., Stark, N.,
786 Gonz√°lez-Quijano, M. and Girardclos, S., 2016. The role of mass-transport
787 deposits and turbidites in shaping modern lacustrine deepwater channels.
788 Marine and Petroleum Geology, 77: 515-525.
789 https://doi.org/10.1016/j.marpetgeo.2016.07.004
790 Coutellier, V., 1985. Mise en évidence et rôle des mouvements gravitaires dans
791 l'évolution de la marge continentale : exemple des marges du Golfe du Lion et de
792 la Provence Occidentale. PhD Thesis, Université Pierre et Marie Curie (Paris VI),
793 197 pp.

Croguennec, C., Ruffine, L., Dennielou, B., Baudin, F.o., Caprais, J.-C., Guyader, V., Bayon, G., Brandily, C., Le Bruchec, J., Bollinger, C., Germain, Y., Droz, L., Babonneau, N. and Rabouille, C., 2017. Evidence and age estimation of mass wasting at the distal lobe of the Congo deep-sea fan. Deep Sea Research Part II: Topical Studies in Oceanography, 142: 50-63. https://doi.org/10.1016/j.dsr2.2016.12.013

De Blasio, F.V. and Elverhøi, A., 2011. Properties of Mass-Transport Deposits as Inferred from Dynamic Modeling of Subaqueous Mass Wasting: A Short Review. In: R.C. Shipp, P. Weimer and H.W. Posamentier (Editors), Mass-Transport Deposits in Deepwater Settings. SEPM Society for Sedimentary Geology. https://doi.org/10.2110/sepmsp.096.499

De Blasio, F.V., Elverhøi, A., Issler, D., Harbitz, C.B., Bryn, P. and Lien, R., 2005. On the dynamics of subaqueous clay rich gravity mass flows—the giant Storegga slide, Norway. Marine and Petroleum Geology, 22(1): 179-186. https://doi.org/10.1016/j.marpetgeo.2004.10.014

Dennielou, B., Droz, L., Babonneau, N., Jacq, C.l., Bonnel, C.d., Picot, M., Le Saout, M., Saout, Y., Bez, M., Savoye, B., Olu, K. and Rabouille, C., 2017. Morphology, structure, composition and build-up processes of the active channel-mouth lobe complex of the Congo deep-sea fan with inputs from remotely operated underwater vehicle (ROV) multibeam and video surveys. Deep Sea Research Part II: Topical Studies in Oceanography, 142: 25-49. https://doi.org/10.1016/j.dsr2.2017.03.010

Dennielou, B., Huchon, A., Beaudouin, C. and Berné, S., 2006. Vertical grain-size variability within a turbidite levee: Autocyclicity or allocyclicity? A case study from the Rhone neofan, Gulf of Lions, Western Mediterranean. Marine Geology, 234(1-4): 191-213. https://doi.org/10.1016/j.margeo.2006.09.019

818 Dennielou, B., Jallet, L., Sultan, N., Jouet, G., Giresse, P., Voisset, M. and Berné, S., 2009.
819 Post-glacial persistence of turbiditic activity within the Rhône deep-sea turbidite
820 system (Gulf of Lions, Western Mediterranean): Linking the outer shelf and the
821 basin sedimentary records. Marine Geology, 257(1-4): 65-86.
822 http://dx.doi.org/10.1016/j.margeo.2008.10.013
823 dos Reis, A.T., Gorini, C. and Mauffret, A., 2005. Implications of salt–sediment
824 interactions on the architecture of the Gulf of Lions deep-water sedimentary
825 systems—western Mediterranean Sea. Marine and Petroleum Geology, 22(6):
826 713-746. https://doi.org/10.1016/j.marpetgeo.2005.03.006
827 Droz, L., 1983. L'éventail sous-marin profond du Rhône (Golfe du lion) : grands traits
828 morphologiques et structure semi-profonde. PhD Thesis, Université Paris VI,
829 Paris, 195 pp. http://archimer.ifremer.fr/doc/00042/15327/
830 Droz, L., 2003. PROGRES cruise, RV Le Suroît. http://dx.doi.org/10.17600/3020080
831 Droz, L. and Bellaiche, G., 1985. Rhone Deep-Sea Fan: morphostructure and growth
832 pattern. American Association of Petroleum Geologists Bulletin, 69: 460-479.
833 Droz, L., Kergoat, R., Cochonat, P. and Berné, S., 2001. Recent sedimentary events in the
834 western Gulf of Lions (Western Mediterranean). Marine Geology, 176(1-4): 23-
835 37. https://doi.org/10.1016/S0025-3227(01)00147-5
836 Droz, L., Reis, A.T.d., Rabineau, M., Berné, S. and Bellaiche, G., 2006. Quaternary turbidite
837 systems on the northern margins of the Balearic Basin (Western Mediterranean):
838 a synthesis. Geo-Marine Letters, 26(6): 347-359.
839 https://doi.org/10.1007/s00367-006-0044-0
840 Dugan, B., 2012. Petrophysical and consolidation behavior of mass transport deposits
841 from the northern Gulf of Mexico, IODP Expedition 308. Marine Geology, 315-
842 318: 98-107. https://doi.org/10.1016/j.margeo.2012.05.001

Gales, J.A., Leat, P.T., Larter, R.D., Kuhn, G., Hillenbrand, C.D., Graham, A.G.C., Mitchell, N.C., Tate, A.J., Buys, G.B. and Jokat, W., 2014. Large-scale submarine landslides, channel and gully systems on the southern Weddell Sea margin, Antarctica. Marine Geology, 348: 73-87. https://doi.org/10.1016/j.margeo.2013.12.002

Garziglia, S., Migeon, S., Ducassou, E., Loncke, L. and Mascle, J., 2008. Mass-transport deposits on the Rosetta province (NW Nile deep-sea turbidite system, Egyptian margin): Characteristics, distribution, and potential causal processes. Marine Geology, 250(3-4): 180-198. https://doi.org/doi:10.1016/j.margeo.2008.01.016

Gaullier, V., 1993. Diapirisme salifère et dynamique sédimentaire dans le bassin liguro-provençal : données sismiques et modèles analogiques. Thèse d'Université Thesis, Université Pierre et Marie Curie (Paris VI), 327 pp. http://archimer.ifremer.fr/doc/00034/14509/

Gaullier, V., Antonini, E., Benkhelil, J. and Got, H., 1998. Recent gravity-driven sedimentary bodies in the North-Balearic Basin: geometry and quantification. Comptes Rendus de l'Academie des Sciences - Series IIA - Earth and Planetary Science, 327(10): 677-684. https://doi.org/10.1016/S1251-8050(99)80025-1

Haflidason, H., Lien, R., Sejrup, H.P., Forsberg, C.F. and Bryn, P., 2005. The dating and morphometry of the Storegga Slide. Marine and Petroleum Geology, 22(1): 123-136. https://doi.org/10.1016/j.marpetgeo.2004.10.008

Hampton, M.A., Lee, H.J. and Locat, J., 1996. Submarine landslides. Reviews of Geophysics, 34(1): 33-59. https://doi.org/10.1029/95RG03287

Hsü, K.J., Cita, M.B. and Ryan, W.B.F., 1973. The origin of the Mediterranean evaporites. In: W.B.F. Ryan and K.J. Hsü (Editors), Leg 13, Init. Rep. Deep Sea Drill. Proj., pp. 1203-1231. https://doi.org/doi:10.2973/dsdp.proc.13.1973

867 Huppertz, T.J., Piper, D.J.W., Mosher, D.C. and Jenner, K., 2010. The Significance of Mass-
868 Transport Deposits for the Evolution of a Proglacial Continental Slope. In: D.C.
869 Mosher et al. (Editors), Submarine Mass Movements and Their Consequences.
870 Springer Netherlands, Dordrecht, pp. 631-641. https://doi.org/10.1007/978-90-
871 481-3071-9_51
872 IFREMER/CIESM, 2011. Morpho-bathymetry of the Mediterranean Sea. QUAE,
873 http://www.quae.com/en/r770-morpho-bathymetry-of-the-mediterranean-
874 sea.html
875 Imbo, Y., De Batist, M., Canals, M., Prieto, M.J. and Baraza, J., 2003. The Gebra Slide: a
876 submarine slide on the Trinity Peninsula Margin, Antarctica. Marine Geology,
877 193(3): 235-252. https://doi.org/10.1016/S0025-3227(02)00664-3
878 Ioualalen, M., Migeon, S. and Sardoux, O., 2010. Landslide tsunami vulnerability in the
879 Ligurian Sea: case study of the 1979 October 16 Nice international airport
880 submarine landslide and of identified geological mass failures. Geophysical
881 Journal International, 181(2): 724-740. https://doi.org/10.1111/j.1365-
882 246X.2010.04572.x
883 Issler, D., De Blasio, F.V., Elverh√∏i, A., Bryn, P. and Lien, R., 2005. Scaling behaviour of
884 clay-rich submarine debris flows. Marine and Petroleum Geology, 22(1): 187-
885 194. https://doi.org/10.1016/j.marpetgeo.2004.10.015
886 Jallet, L. and Giresse, P., 2005. Construction of the Pyreneo-Languedocian Sedimentary
887 Ridge and associated sediment waves in the deep western Gulf of Lions (Western
888 Mediterranean). Marine and Petroleum Geology, 22(6-7): 865-888.
889 https://doi.org/10.1016/j.marpetgeo.2005.03.008
890 Jansen, E., Befring, S., Bugge, T., Eidvin, T., Holtedahl, H. and Sejrup, H.P., 1987. Large
891 submarine slides on the Norwegian continental margin: Sediments, transport and

timing. Marine Geology, 78(1): 77-107. https://doi.org/10.1016/0025-3227(87)90069-7

Jégou, I., 2008. Etude de la transition chenal-levées/lobes dans les systèmes turbiditiques récents : Application à l'éventail turbiditique de l'Amazone et au Néofan du Petit-Rhône. Doctorat Thesis, Université de Brest, Brest, 350 pp. http://archimer.ifremer.fr/doc/00000/6796/

Joanne, C., Collot, J.-Y., Lamarche, G. and Migeon, S.b., 2010. Continental slope reconstruction after a giant mass failure, the example of the Matakaoa Margin, New Zealand. Marine Geology, 268(1): 67-84. https://doi.org/10.1016/j.margeo.2009.10.013

Jouet, G., Berne, S., Rabineau, M., Bassetti, M.A., Bernier, P., Dennielou, B., Sierro, F.J., Flores, J.A. and Taviani, M., 2006. Shoreface migrations at the shelf edge and sea-level changes around the Last Glacial Maximum (Gulf of Lions, NW Mediterranean). Marine Geology, 234(1-4): 21-42. https://doi.org/10.1016/j.margeo.2006.09.012

Kawamura, K., Kanamatsu, T., Kinoshita, M., Saito, S., Shibata, T., Fujino, K., Misawa, A. and Burmeister, K.C., 2010. Redistribution of Sediments by Submarine Landslides on the Eastern Nankai Accretionary Prism. In: D.C. Mosher et al. (Editors), Submarine Mass Movements and Their Consequences. Springer Netherlands, Dordrecht, pp. 313-322. https://doi.org/10.1007/978-90-481-3071-9_26

Kelner, M., Migeon, S., Tric, E., Couboulex, F., Dano, A. and Lebourg, T., 2014. Recent Morphological Changes of the Nice Continental Slope. In: G. Lollino, A. Manconi, J. Locat, Y. Huang and M. Canals Artigas (Editors), Engineering Geology for Society and Territory. Springer, Cham, 4, pp. 221-225. https://doi.org/10.1007/978-3-319-08660-6_42

Kneller, B., Dykstra, M., Fairweather, L. and Milana, J.P., 2016. Mass-transport and slope accommodation: Implications for turbidite sandstone reservoirs. AAPG Bulletin, 100(2): 213-235.

Lastras, G., Canals, M., Amblas, D., Frigola, J., Urgeles, R., Calafat, A.M. and Acosta, J., 2007a. Slope instability along the northeastern Iberian and Balearic continental margins. Geologica Acta: an international earth science journal, 5(1): 35-48. http://www.redalyc.org/articulo.oa?id=50550103

Lastras, G., Canals, M., Hughes-Clarke, J.E., Moreno, A., De Batist, M., Masson, D.G. and P., C., 2002. Seafloor imagery from the BIG'95 debris flow, western Mediterranean. Geology, 30(10): 871-874. https://doi.org/10.1130/0091-7613(2002)030%3C0871:SIFTBD%3E2.0.CO;2

Lastras, G., Canals, M., Urgeles, R., Amblas, D., Ivanov, M., Droz, L., Dennielou, B., Fabres, J., Schoolmeester, T., Akhmetzhanov, A., Orange, D. and Garcia-Garcia, A., 2007b. A walk down the Cap de Creus canyon, Northwestern Mediterranean Sea: Recent processes inferred from morphology and sediment bedforms. Marine Geology, 246(2-4): 176-192. https://doi.org/10.1016/j.margeo.2007.09.002

Lastras, G., Canals, M., Urgeles, R., De Batist, M., Calafat, A.M. and Casamor, J.L., 2004. Characterisation of the recent BIG'95 debris flow deposit on the Ebro margin, Western Mediterranean Sea, after a variety of seismic reflection data. Marine Geology, 213(1): 235-255. https://doi.org/10.1016/j.margeo.2004.10.008

Le Cann, C., 1987. Le diapirisme dans le bassin Liguro-provençal (Méditerranée occidentale). Relations avec la tectonique et la sédimentation. Implications géodynamiques. Université de Bretagne Occidentale, Brest, 296 pp. http://archimer.ifremer.fr/doc/00034/14519/

941 Lee, H.J., 2009. Timing of occurrence of large submarine landslides on the Atlantic Ocean
942 margin. Marine Geology, 264(1-2): 53-64.
943 https://doi.org/10.1016/j.margeo.2008.09.009
944 Leroux, E., Rabineau, M., Aslanian, D., Gorini, C., Molliex, S., Bache, F., Robin, C., Droz, L.,
945 Moulin, M., Poort, J., Rubino, J.-L. and Suc, J.-P., 2017. High-resolution evolution of
946 terrigenous sediment yields in the Provence Basin during the last 6 Ma: relation
947 with climate and tectonics. Basin research, 29(3): 305-339.
948 https://doi.org/10.1111/bre.12178
949 Leroux, E., Rabineau, M., Aslanian, D., Granjeon, D., Droz, L. and Gorini, C., 2014.
950 Stratigraphic simulations of the shelf of the Gulf of Lions: testing subsidence rates
951 and sea,Äêlevel curves during the Pliocene and Quaternary. Terra Nova, 26(3):
952 230-238. https://doi.org/10.1111/ter.12091
953 Lofi, J., Rabineau, M., Gorini, C., Berne, S., Clauzon, G., De Clarens, P., Dos Reis, A.T.,
954 Mountain, G.S., Ryan, W.B.F., Steckler, M.S. and Fouchet, C., 2003. Plio-Quaternary
955 prograding clinoform wedges of the western Gulf of Lion continental margin (NW
956 Mediterranean) after the Messinian Salinity Crisis. Marine Geology, 198(3-4):
957 289-317. https://doi.org/10.1016/s0025-3227(03)00120-8
958 Lombo Tombo, S., Dennielou, B., Berné, S., Bassetti, M.A., Toucanne, S., Jorry, S.J., Jouet, G.
959 and Fontanier, C., 2015. Sea-level control on turbidite activity in the Rhone
960 canyon and the upper fan during the Last Glacial Maximum and Early deglacial.
961 Sedimentary Geology, 323(0): 148-166.
962 http://dx.doi.org/10.1016/j.sedgeo.2015.04.009
963 Loubrieu, B., 1997. CALMAR97 cruise, RV L'Atalante.
964 http://dx.doi.org/10.17600/97010120

965 Maldonado, A., Palanques, A., Alonso, B., Kastens, K.A., Nelson, C.H., O'Connell, S. and
966 Ryan, W.B.F., 1985. Physiography and deposition on a distal deep-sea system:
967 The Valencia Fan (Northwestern Mediterranean). Geo-marine letters, 5(3): 157-
968 164. https://doi.org/10.1007/bf02281633
969 Manchuel, K., Traversa, P., Baumont, D., Cara, M., Nayman, E. and Durouchoux, C., 2017.
970 The French seismic CATalogue (FCAT-17). Bulletin of Earthquake Engineering.
971 http://dx.doi.org/10.1007/s10518-017-0236-1
972 Mauffrey, M.A., Berné, S., Jouet, G., Giresse, P. and Gaudin, M., 2015. Sea-level control on
973 the connection between shelf-edge deltas and the Bourcart canyon head (western
974 Mediterranean) during the last glacial/interglacial cycle. Marine Geology, 370: 1-
975 19. http://dx.doi.org/10.1016/j.margeo.2015.09.010
976 Mazières, A., Gillet, H., Castelle, B., Mulder, T., Guyot, C., Garlan, T. and Mallet, C., 2014.
977 High-resolution morphobathymetric analysis and evolution of Capbreton
978 submarine canyon head (Southeast Bay of Biscay—French Atlantic Coast) over
979 the last decade using descriptive and numerical modeling. Marine Geology, 351:
980 1-12. https://doi.org/10.1016/j.margeo.2014.03.001
981 McHugh, C.M.G., Damuth, J.E., Gartner, S., Katz, M.E. and Mountain, G.S., 1996. Oligocene
982 to Holocene mass-transport deposits of the New Jersey continental margin and
983 their correlation to sequence boundaries. In: G.S. Mountain, K.G. Miller, P. Blum,
984 C.W. Poag and D.C. Twichell (Editors), Proceedings of the Ocean Drilling Program,
985 Scientific Results, 150, pp. 189-228.
986 http://dx.doi.org/10.2973/odp.proc.sr.150.016.1996
987 Méar, Y. and Gensous, B., 1993. Processus d'édification d'une unite interlobe; application
988 au deep-sea fan du Petit-Rhône. Comptes Rendus de l'Académie des Sciences,

989 Serie II, Mécanique, Physique, Chimie, Sciences de l'Univers, Sciences de la Terre,
990 317(12): 1633-1640.
991 Melki, T., Kallel, N., Jorissen, F.J., Guichard, F., Dennielou, B., Berné, S., Labeyrie, L. and
992 Fontugne, M., 2009. Abrupt climate change, sea surface salinity and
993 paleoproductivity in the western Mediterranean Sea (Gulf of Lion) during the last
994 28 kyr. Palaeogeography, Palaeoclimatology, Palaeoecology, 279(1-2): 96-113.
995 https://doi.org/10.1016/j.palaeo.2009.05.005
996 Micallef, A., Mountjoy, J.J., Canals, M. and Lastras, G., 2012. Deep-Seated Bedrock
997 Landslides and Submarine Canyon Evolution in an Active Tectonic Margin: Cook
998 Strait, New Zealand. In: Y. Yamada et al. (Editors), Submarine Mass Movements
999 and Their Consequences. Springer Netherlands, Dordrecht, pp. 201-212.
1000 https://doi.org/10.1007/978-94-007-2162-3_18
1001 Migeon, S., Cattaneo, A., Hassoun, V., Larroque, C., Corradi, N., Fanucci, F., Dano, A., de
1002 Lepinay, B.M., Sage, F. and Gorini, C., 2011. Morphology, distribution and origin of
1003 recent submarine landslides of the Ligurian Margin (North-western
1004 Mediterranean): some insights into geohazard assessment. Marine Geophysical
1005 Research, 32(1-2): 225-243. https://doi.org/10.1007/s11001-011-9123-3
1006 Mohrig, D., Ellis, C., Parker, G., Whipple, K.X. and Hondzo, M., 1998. Hydroplaning of
1007 subaqueous debris flows. GSA Bulletin, 110(3): 387-394.
1008 https://doi.org/10.1130/0016-7606(1998)110<0387:HOSDF>2.3.CO;2
1009 Mulder, T., 2011. Chapter 2 - Gravity Processes and Deposits on Continental Slope, Rise
1010 and Abyssal Plains. In: H. HüNeke and T. Mulder (Editors), Developments in
1011 Sedimentology. Elsevier, 63, pp. 25-148. https://doi.org/10.1016/B978-0-444-
1012 53000-4.00002-0

1013 Mulder, T. and Cochonat, P., 1996. Classification of offshore mass movements, Journal of
1014 Sedimentary Research, pp. 43-57.
1015 Nelson, C.H., Escutia, C., Damuth, J.E. and Twichell, J.D.C., 2011. Interplay of Mass-
1016 Transport and Turbidite-System Deposits in Different Active Tectonic and
1017 Passive Continental Margin Settings: External and Local Controlling Factors. In:
1018 R.C. Shipp, P. Weimer and H.W. Posamentier (Editors), Mass-Transport Deposits
1019 in Deepwater Settings. SEPM Society for Sedimentary Geology, pp. 39-66.
1020 https://doi.org/10.2110/sepmsp.096.039
1021 O'Connell, S., Normark, W.R., Ryan, W.B.F. and Kenyon, N.H., 1991. An entrenched
1022 thalweg channel on the Rhône fan : interpretation from a SEABEAM and
1023 SEAMARC I survey, SEPM Special Publication, 46, pp. 259-270.
1024 https://doi.org/10.2110/pec.91.09.0259
1025 Obelcz, J., Xu, K., Georgiou, I.Y., Maloney, J., Bentley, S.J. and Miner, M.D., 2017. Sub-
1026 decadal submarine landslides are important drivers of deltaic sediment flux:
1027 Insights from the Mississippi River Delta Front. Geology, 45(8): 703-706.
1028 https://doi.org/10.1130/G38688.1
1029 Ortiz-Karpf, A., Hodgson, D.M. and McCaffrey, W.D., 2015. The role of mass-transport
1030 complexes in controlling channel avulsion and the subsequent sediment
1031 dispersal patterns on an active margin: The Magdalena Fan, offshore Colombia.
1032 Marine and Petroleum Geology, 64: 58-75.
1033 https://doi.org/10.1016/j.marpetgeo.2015.01.005
1034 Ouimet, W.B., Whipple, K.X., Royden, L.H., Sun, Z. and Chen, Z., 2007. The influence of
1035 large landslides on river incision in a transient landscape: Eastern margin of the
1036 Tibetan Plateau (Sichuan, China). GSA Bulletin, 119(11-12): 1462-1476.
1037 https://doi.org/10.1130/B26136.1

1038 Palanques, A., Durrieu de Madron, X., Puig, P., Fabres, J., Guillen, J., Calafat, A., Canals, M.,
1039 Heussner, S. and Bonnin, J., 2006. Suspended sediment fluxes and transport
1040 processes in the Gulf of Lions submarine canyons. The role of storms and dense
1041 water cascading. Marine Geology, 234(1-4): 43-61.
1042 https://doi.org/10.1016/j.margeo.2006.09.002
1043 Palanques, A., Puig, P., Latasa, M. and Scharek, R., 2009. Deep sediment transport
1044 induced by storms and dense shelf-water cascading in the northwestern
1045 Mediterranean basin. Deep Sea Research Part I: Oceanographic Research Papers,
1046 56(3): 425-434. https://doi.org/10.1016/j.dsr.2008.11.002
1047 Payo-Payo, M., Jacinto, R.S., Lastras, G., Rabineau, M., Puig, P., Martín, J., Canals, M. and
1048 Sultan, N., 2017. Numerical modeling of bottom trawling-induced sediment
1049 transport and accumulation in La Fonera submarine canyon, northwestern
1050 Mediterranean Sea. Marine Geology, 386: 107-125.
1051 https://doi.org/10.1016/j.margeo.2017.02.015
1052 Piper, D., Pirmez, C., Manley, L.P., Long, D., Flood, R.D., Normark, W. and Showers, W.,
1053 1997. Mass-transport deposits of the Amazon Fan. In: R.D. Flood, D. Piper, A.
1054 Klaus and L.C. Peterson (Editors), Proceedings of the Ocean Drilling Program,
1055 Scientific Results, 155, College Station TX, pp. 109-146.
1056 http://dx.doi.org/doi:10.2973/odp.proc.sr.155.212.1997
1057 Piper, D.J.W., Mosher, D.C., Gauley, B.J., Jenner, K. and Campbell, D.C., 2003. The
1058 Chronology and Recurrence of Submarine Mass Movements on the Continental
1059 Slope Off Southeastern Canada. In: J. Locat, J.. Mienert and L. Boisvert (Editors),
1060 Submarine Mass Movements and Their Consequences: 1st International
1061 Symposium. Springer Netherlands, Dordrecht, pp. 299-306.
1062 https://doi.org/10.1007/978-94-010-0093-2_33

1063 Pont, D., Simonnet, J.-P. and Walter, A.V., 2002. Medium-term Changes in Suspended
1064 Sediment Delivery to the Ocean: Consequences of Catchment Heterogeneity and
1065 River Management (Rhone River, France). Estuarine, Coastal and Shelf Science,
1066 54(1): 1-18. https://doi.org/10.1006/ecss.2001.0829
1067 Popescu, I., Lericolais, G., Panin, N., Wong, H.K. and Droz, L., 2001. Late Quaternary
1068 channel avulsions on the Danube deep-sea fan, Black Sea. Marine Geology, 179(1-
1069 2): 25-37. https://doi.org/10.1016/S0025-3227(01)00197-9
1070 Rabineau, M. and Aslanian, D., 2007. SEEPGOL cruise, RV Le Suroît.
1071 http://dx.doi.org/10.17600/7020080
1072 Rabineau, M., Berne, S., Aslanian, D., Olivet, J.-L., Joseph, P., Guillocheau, F., Bourillet, J.-F.,
1073 Ledrezen, E. and Granjeon, D., 2005. Sedimentary sequences in the Gulf of Lion: A
1074 record of 100,000 years climatic cycles. Marine and Petroleum Geology, 22(6-7):
1075 775-804. https://doi.org/10.1016/j.marpetgeo.2005.03.010
1076 Rabineau, M., Berne, S., Ledrezen, E., Lericolais, G., Marsset, T. and Rotunno, M., 1998. 3D
1077 architecture of lowstand and transgressive Quaternary sand bodies on the outer
1078 shelf of the Gulf of Lion, France. Marine and Petroleum Geology, 15(5): 439-452.
1079 Rabineau, M., Berne, S., Olivet, J.-L., Aslanian, D., Guillocheau, F. and Joseph, P., 2006.
1080 Paleo sea levels reconsidered from direct observation of paleoshoreline position
1081 during Glacial Maxima (for the last 500,000 yr). Earth and Planetary Science
1082 Letters, 252(1-2): 119-137. https://doi.org/10.1016/j.epsl.2006.09.033
1083 Rabineau, M., Leroux, E., Aslanian, D., Bache, F., Gorini, C., Moulin, M., Molliex, S., Droz, L.,
1084 dos Reis, A.T., Rubino, J.L., Guillocheau, F. and Olivet, J.L., 2014. Quantifying
1085 subsidence and isostatic readjustment using sedimentary paleomarkers, example
1086 from the Gulf of Lion. Earth and planetary science letters, 388: 353-366.
1087 https://doi.org/10.1016/j.epsl.2013.11.059

1088 Reeder, M.S., Rothwell, R.G. and Stow, D.A.V., 2000. Infuence of sea level and basin
1089 physiography on emplacement of the late Pleistocene Herodotus Basin
1090 Megaturbidite, SE Mediterranean Sea. Marine and Petroleum Geology, 17(2):
1091 199-218. https://doi.org/10.1016/S0264-8172(99)00048-3
1092 Reimer, P.J., Bard, E., Bayliss, A., Beck, J.W., Blackwell, P.G., Ramsey, C.B., Buck, C.E.,
1093 Cheng, H., Edwards, R.L., Friedrich, M., Grootes, P.M., Guilderson, T.P., Haflidason,
1094 H., Hajdas, I., Hatte, C., Heaton, T.J., Hoffmann, D.L., Hogg, A.G., Hughen, K.A.,
1095 Kaiser, K.F., Kromer, B., Manning, S.W., Niu, M., Reimer, R.W., Richards, D.A., Scott,
1096 E.M., Southon, J.R., Staff, R.A., Turney, C.S.M. and van der Plicht, J., 2013. Intcal13
1097 and Marine13 radiocarbon age calibration curves 0-50,000 Years Cal BP.
1098 Radiocarbon, 55(4): 1869-1887. https://doi.org/10.2458/azu_js_rc.55.16947
1099 Rothwell, R.G., Reeder, M.S., Anastasakis, G., Stow, D.A.V., Thomson, J. and Kähler, G.,
1100 2000. Low sea-level stand emplacement of megaturbidites in the western and
1101 eastern Mediterranean Sea. Sedimentary Geology, 135(1-4): 75-88.
1102 https://doi.org/10.1016/S0037-0738(00)00064-6
1103 Rothwell, R.G., Thomson, J. and Kähler, G., 1998. Low-sea-level emplacement of a very
1104 large Late Pleistocene 'megaturbidite' in the western Mediterranean Sea. Nature,
1105 392(6674): 377-380. https://doi.org/10.1038/32871
1106 San Pedro, L., Babonneau, N., Gutscher, M.A. and Cattaneo, A., 2017. Origin and
1107 chronology of the Augias deposit in the Ionian Sea (Central Mediterranean Sea),
1108 based on new regional sedimentological data. Marine Geology, 384: 199-213.
1109 https://doi.org/10.1016/j.margeo.2016.05.005
1110 Shanmugam, G. and Wang, Y., 2015. The landslide problem. Journal of Palaeogeography,
1111 4(2): 109-166. http://dx.doi.org/10.3724/SP.J.1261.2015.00071

1112 Shipp, R.C., Weimer, P. and Posamentier, H.W., 2011. Mass-Transport Deposits in
1113 Deepwater Settings: An Introduction. In: R.C. Shipp, P. Weimer and H.W.
1114 Posamentier (Editors), Mass-Transport Deposits in Deepwater Settings. SEPM
1115 Society for Sedimentary Geology. https://doi.org/10.2110/sepmsp.096.003
1116 Shugar, D.H., Clague, J.J., Best, J.L., Schoof, C., Willis, M.J., Copland, L. and Roe, G.H., 2017.
1117 River piracy and drainage basin reorganization led by climate-driven glacier
1118 retreat. Nature Geoscience, 10: 370. https://doi.org/10.1038/ngeo2932
1119 Sierro, F.J., Andersen, N., Bassetti, M.A., BernÈ, S., Canals, M., Curtis, J.H., Dennielou, B.,
1120 Flores, J.A., Frigola, J., Gonzalez-Mora, B., Grimalt, J.O., Hodell, D.A., Jouet, G.,
1121 PÈrez-Folgado, M. and Schneider, R., 2009. Phase relationship between sea level
1122 and abrupt climate change. Quaternary Science Reviews, 28(25-26): 2867-2881.
1123 https://doi.org/10.1016/j.quascirev.2009.07.019
1124 Skinner, L.C. and McCave, I.N., 2003. Analysis and modelling of gravity- and piston coring
1125 based on soil mechanics. Marine Geology, 199(1-2): 181-204.
1126 https://doi.org/10.1016/S0025-3227(03)00127-0
1127 Smith, D.P., Kvitek, R., Iampietro, P.J. and Wong, K., 2007. Twenty-nine months of
1128 geomorphic change in upper Monterey Canyon (2002,Äì2005). Marine Geology,
1129 236(1): 79-94. https://doi.org/10.1016/j.margeo.2006.09.024
1130 Stabholz, M., Durrieu de Madron, X., Canals, M., Khripounoff, A., Taupier-Letage, I.,
1131 Testor, P., Heussner, S., Kerhervé, P., Delsaut, N., Houpert, L., Lastras, G. and
1132 Dennielou, B., 2013. Impact of open-ocean convection on particle fluxes and
1133 sediment dynamics in the deep margin of the Gulf of Lions. Biogeosciences, 10(2):
1134 1097-1116. https://doi.org/10.5194/bg-10-1097-2013
1135 Stuiver, M., Reimer, P.J. and Reimer, R.W., 2018. CALIB 7.1 [WWW program].
1136 http://calib.org.

Sultan, N., Gaudin, M., Berne, S., Canals, M., Urgeles, R. and Lafuerza, S., 2007. Analysis of slope failures in submarine canyon heads: An example from the Gulf of Lions. Journal of Geophysical Research, 112(F01009). http://dx.doi.org/doi:10.1029/2005JF000408

Sultan, N. and Voisset, M., 2002. GMO2 - CARNAC cruise, RV Le Suroît. http://dx.doi.org/10.17600/2020080

Tesson, M. and Gensous, B., 1998. L'enregistrement des cycles climatiques et eustatiques quaternaires de marges récentes du bassin Nord-Méditerranéen ; Quaternary record of climatic and eustatic cycles on modem margins of the north-mediterranean basin. Comptes Rendus de l'Académie des Sciences - Series IIA - Earth and Planetary Science, 326(2): 121-127. https://doi.org/10.1016/S1251-8050(97)87456-3

Torres, J., Droz, L., Savoye, B., Terentieva, E., Cochonat, P., Kenyon, N.H. and Canals, M., 1997. Deep-sea avulsion and morphosedimentary evolution of the Rhône Fan Valley and Neofan during the Late Quaternary (north-western Mediterranean Sea). Sedimentology, 44: 457-477. https://doi.org/10.1046/j.1365-3091.1997.d01-36.x

Torres, J., Savoye, B. and Cochonat, P., 1995. The effects of late quaternary sea-level changes on the Rhône slope sedimentation (northwestern mediterranean), as indicated by seismic stratigraphy. Journal of Sedimentary Research, B65(3): 368-387. https://doi.org/10.1306/D4268257-2B26-11D7-8648000102C1865D

Tripsanas, E.K., Piper, D.J.W., Jenner, K.A. and Bryant, W.R., 2008. Submarine mass-transport facies: new perspectives on flow processes from cores on the eastern North American margin. Sedimentology, 55: 97-136. doi:10.1111/j.1365-3091.2007.00894.x

Turon, J.-L., 2001. MD 123 / GEOSCIENCES 1 cruise, RV Marion Dufresne. http://dx.doi.org/10.17600/1200050

Twichell, D.C., Kenyon, N.H., Parson, L.M. and McGregor, B.A., 1991. Depositional Patterns of the Mississippi Fan Surface: Evidence from GLORIA II and High-Resolution Seismic Profiles. In: P. Weimer and M.H. Link (Editors), Seismic Facies and Sedimentary Processes of Submarine Fans and Turbidite Systems. Springer New York, New York, NY, pp. 349-363. http://dx.doi.org10.1007/978-1-4684-8276-8_19

Urgeles, R. and Camerlenghi, A., 2013. Submarine landslides of the Mediterranean Sea: Trigger mechanisms, dynamics, and frequency-magnitude distribution. Journal of Geophysical Research: Earth Surface, 118(4): 2600-2618. http://dx.doi.org/10.1002/2013jf002720

Weimer, P., 1989. Sequence stratigraphy of the Mississippi fan (Plio-Pleistocene), Gulf of Mexico. Geo-marine letters, 9(4): 185-272. https://doi.org/10.1007/bf02431072

Figure captions

Figure 1

Bathymetric map of the Gulf of Lions and Catalan margins with indication of main morpho-sedimentary features (white dashed lines: sedimentary deposits; black dashed lines: Mass Transport Deposits; violet dashed lines: main canyons; black solid line: current Petit-Rhone canyon/channel). Gulf of Lions canyons (Berné et al., 2004): CC: Cap de Creus, LD: Lacaze Duthier, P: Pruvost, Bc: Bourcart, He: Herault, S: Sète, CL: Catherine Laurence, M: Marti (whose coalescence forms the Sète canyons network), PR: Petit-Rhone, GR: Grand-Rhone, Ms: Marseille, PL: Planier, C: Cassidaigne. Catalan margin canyons (Canals et al., 1983): LF: La Fonera, CdP: Clots del Puget, B: Blanes. REMTD:

Eastern Mass Transport Deposit, RWMTD: Western Mass Transport Deposit. Limits of sedimentary bodies are from Droz et al. (2006) except Valencia Fan from Maldonado et al. (1985).

Figure 2

Location map of slides headwalls, of buried and active listric faults (dos Reis et al., 2005), of seismic lines shown in Figs 5 to 9 and of sediment cores (white dots). PLSR: Pyreneo-Langudocian Sedimentary Ridge, PRDSF: Petit-Rhone Deep-Sea Fan, PRN: Petit-Rhone Neofan, REMTD: Eastern Mass Transport Deposit, RWMTD: Western Mass Transport Deposit. See Fig. 1 for canyon names.

Figure 3

Location map of used seismic data and sediment cores

Figure 4

A: Seabed morphology of the study area (map of slope) with location seismic lines and sediment cores. B: zoom in on the seabed morphology on the proximal area of the Western Mass Transport Deposit (RWMTD) at the base of slope. See scars headwall superimposed on active listric faults. Thick red arrows indicate possible main sources and pathways of the RWMTD across the western levee of the Rhone fan. C: zoom in on the seabed morphology of the eastern distal area of the RWMTD showing a bulge against the Rhone fan. D: Bathymetric section A-A' and B-B' show the morphologic expression of the compression bulge. C: bathymetric sections across the Sète valley (A-A'), showing the compression bulge at the contact between the RWMTD and the Rhone fan (B-B' and C-C'). See Figs. 2 and 4A for location. PLSR: Pyreneo-Langudocian Sedimentary Ridge.

Figure 5

The Rhone Western Mass Transport Deposit (RWMTD) as seen by several types of seismic: (A and C) single channel mini GI air-gun, (B) 24-channel mini-GI air-gun, (D) 6-channel 50 Hz GI air-gun, in the proximal area at the base of slope; strike lines (A, B, C), dip lines (D). Lines A and B were acquired simultaneously but with two different streamers. See the nearly transparent facies of the RWMTD on the single channel air-gun line (A) while on the 24-channel air-gun line (B) it shows internal reflections. See Figs. 2 and 4A for lines location. The top (red line) and base (blue line) of the RWMTD in D are issued from the interpretation of sub-bottom profiles. PLSR: Pyreneo-Langudocian Sedimentary Ridge.

Figure 6

Sub-Bottom Profiler lines (A) across the Rhone fan valley and proximal area of the Rhone Western Mass Transport Deposit (RWMTD) showing sliding of the turbiditic levee, and (B) along the central and distal area of the RWMTD. See also location and penetration of sediment cores on the RWMTD. See Figs. 2 and 4A for lines location.

Figure 7

Sub-Bottom Profiler (A) and air gun (B) seismic line across the central area of the Rhone Western Mass Transport Deposit (RWMTD). See overlapping more recent deposits and erosional features (Rhone neofan deposits and channels, scours field and deposits from La Fonera canyon). The top (red line) and base (blue line) of the RWMTD are indicated. See Fig. 2 and 4A for lines location.

Figure 8

Sub-Bottom Profiler line across the distal area of the Rhone Western Mass Transport Deposit (RWMTD). See infill of substratum relief (A), overlap of RWMTD on the Rhone fan (B), infill of Palamos valley (C) and confluence of Clots del Puget/Entrant de Palamós and Valencia valleys. The top (red line) and base (blue line) of the RWMTD are indicated. See Figs. 2 and 4A for lines location.

Figure 9

Sub-Bottom Profiler line across the eastern side of the Rhone Western Mass Transport Deposit (RWMTD) showing overlapping and a compression bulge against the Rhone fan. The top (red line) and base (blue line) of the RWMTD are indicated. See Figs. 2 and 4A for lines location.

Figure 10

Set of maps obtained after interpretation of seismic lines. A: isochron map converted into meters below seafloor of the top of the Rhone Western Mass Transport Deposit (RWMTD). White lines outline deposits that overlap the RWMTD, thick lines: Pyreneo-Langudocian Sedimentary Ridge (PLSR) and neofan, thin lines the Sète and La Fonera lobes (Droz et al., 2001). B: isochron map converted into meters below seafloor of the base of the RWMTD. White arrows outline the presently buried valleys in the prolongation of the Sète canyon. Blue dotted line (A-A') shows the location of depth profiles shown on D. C: isochore map of the RWMTD. D: Depth profiles along the buried valley in the prolongation of the Sète canyon; red: base of the RWMTD; blue: top of the RWMTD; black: present bathymetry. Listric faults (LF) offsets are visible on the bathymetry profile at the base of slope, in the RWMTD proximal area.

Figure 11

Lithofacies of sediment cores collected in the Rhone Western Mass Transport Deposit (RWMTD) at proximal (core MD01-2435), central (core KSGC-10) and distal (core MD01-2438) locations. See Figs 2, 3 and 4A for location of sediment cores.

Figure 12

Graphic presentation of radiocarbon dating at the base of the hemipelagic drape on top of the Rhone Western Mass Transport Deposit (RWMTD) (this paper) and of the Balearic Abyssal Plain Megabed (Rothwell et al., 1998).

Figure 13

Reconstruction maps of canyons and turbidic channels drainage network and sediment routing during the Last Glacial Maximum (LGM), before (A) and after (B) the emplacement of the Rhone Western Mass Transport Deposit (RWMTD). Solid black line indicated location of the buried valley as mapped from seimic lines. Dashed black lines indicate possible location of another parallel valley and areas where the lack of seimic lines do not allow mapping the buried valley. See Fig. 1 for canyon names.

Table captions

Table 1

Oceanographic campaigns and data used in this study. See location in Fig. 3

Table 2

1286 Location and characteristics of sediment cores used in this study. See Figs. 2 and 3 for
1287 location.
1288
1289 *Table 3*
1290 Radiocarbon dating carried out on sediment cores. Calendar ages BP (Before Present)
1291 calculated with Calib 7.1 and Marine13 calibration curve (Reimer et al., 2013). ΔR = 48 y
1292 ; SD = 101 y was determined after reservoir ages in the Gulf of Lions obtained from Calib
1293 7.1 marine reservoir database.
1294

1295 Table 1

Campaign	**Year**	**Ship**	**Data**	**Reference**
Calmar97	1997	R/V L'Atalante	EM12, HR 6-channel 50 Hz GI, VHR 3.5 kHz SBP	(Loubrieu, 1997)
Marion	2000	R/V Le Suroît	EM300, HR single channel and 24 channels 130 Hz mini-GI	(Berné, 2000)
Gmo1	2001	R/V Le Suroît	EM300	(Cochonat, 2001)
MD123 / Geoscience1	2001	R/V Marion Dufresne	Calypso cores	(Turon, 2001)
Gmo2-Carnac	2002	R/V Le Suroît	EM300	(Sultan and Voisset, 2002)
Progres	2003	R/V Le Suroît	EM300, HR 6-channel 50 Hz GI, VHR 2-5.2 kHz SBP	(Droz, 2003)
Sardinia	2006	R/V L'Atalante	EM12, VHR 3.5 kHz SBP	(Aslanian et al., 2006)
Melrose Seepgol	2007	R/V Le Suroît	EM300	(Rabineau and Aslanian, 2007)
Rhosos	2008	R/V Le Suroît	EM300, VHR 2-5.2 kHz SBP	(Berné and Dennielou, 2008)

1296

1297

1298 Table 2

Core	Area	Latitude	Longitude	Water depth (m)	Length (m)	IGSN
MD01-2435	Proximal area	42°15.66' N	004°47.18' E	2025	19.23	BFBGX-88347
KSGC-10	Central area	41° 55.277'N	004 44.608' E	2399	2.03	BFBGX-87938
MD01-2438	Distal area	41°14.91' N	004°29.97' E	2628	9.00	BFBGX-88349

1299

1300

1301 Table 3

Core	Depth (cm)	Radiocarbon age (y BP)	1σ calendar age (y BP)	2 σ calendar age (y BP)	Median calendar age (y BP)	Dated material	Lab. number
MD01-2435	22-24	12,940±70	14,379-14,980	14,163-15,134	14,666	*G. bulloides*	Poz-14639
MD01-2435	853-858	17,940±90	20,921-21,331	20,726-21,535	21,128	*G. bulloides*	Poz-14641
MD01-2435	917-923	18,310±90	21,450-21,825	21,194-21,981	21,625	*G. bulloides*	Poz-14642
MD01-2438	96-100	17,260±80	20,110-20,446	19,949-20,600	20,276	*G. bulloides*	Poz-14649
KSGC-10	1-2	840±30	318-499	239-621	415	*G. bulloides*	Poz-13817

1302

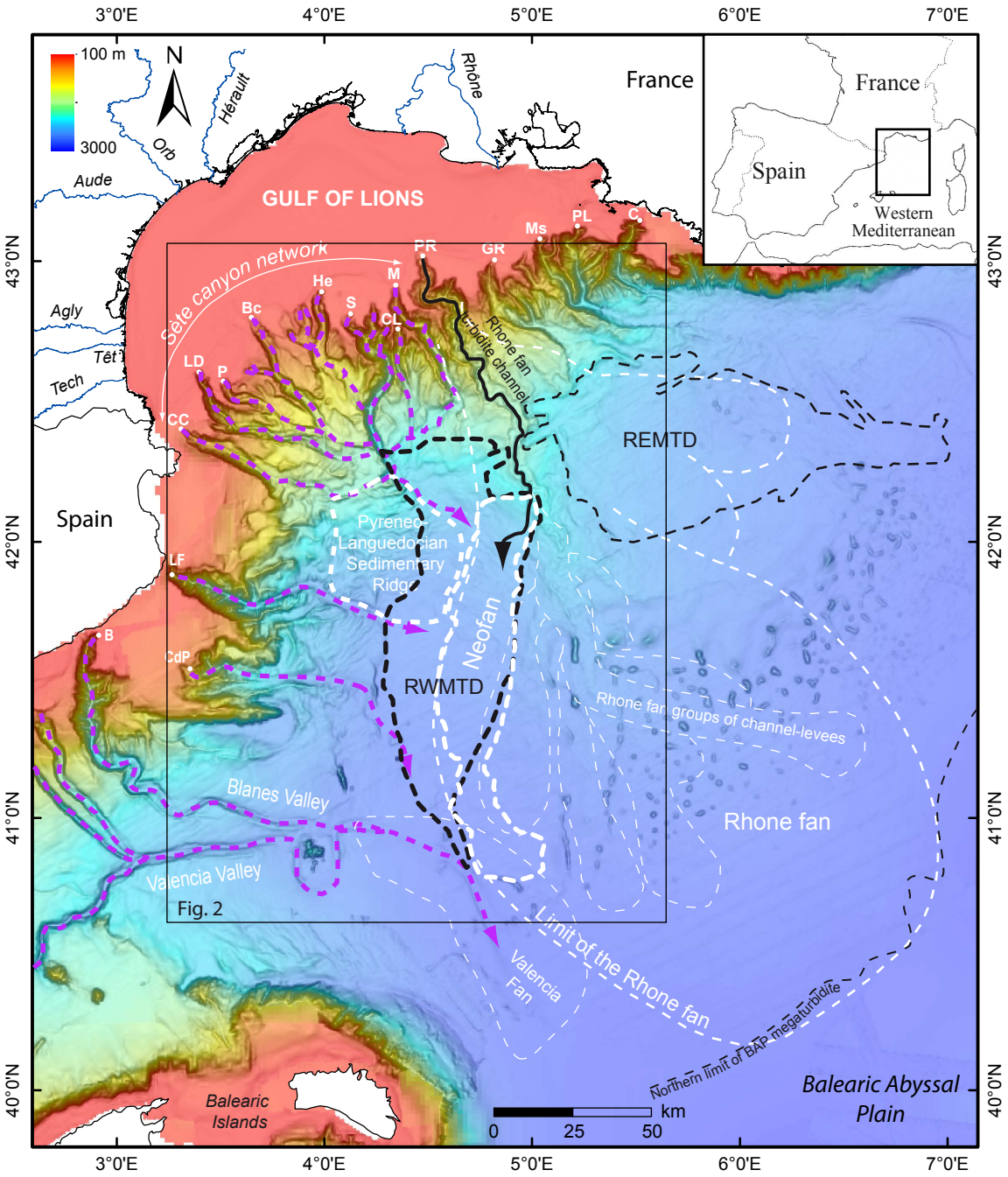

Dennielou et al. RWMTD - Figure 1

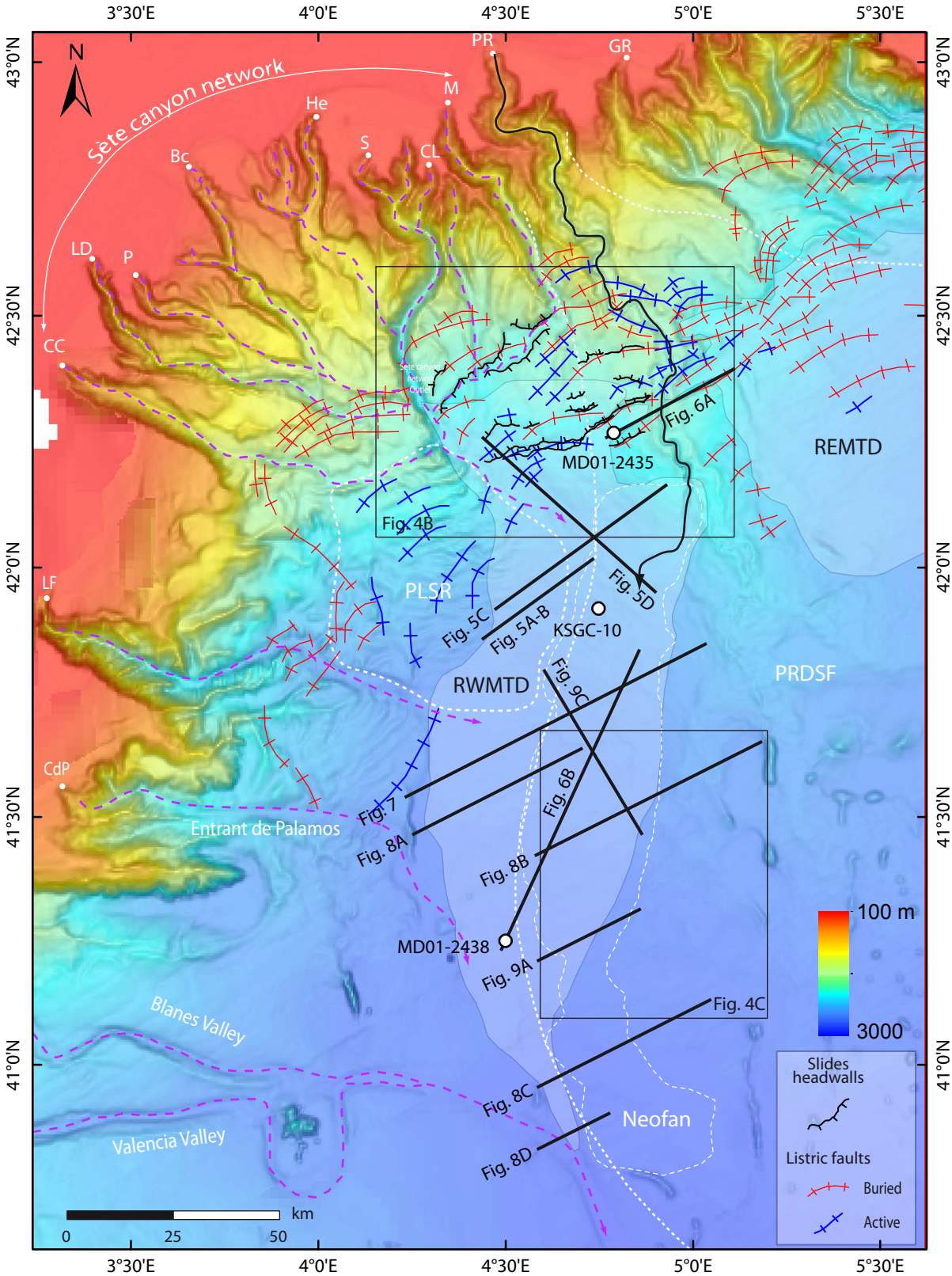

Dennielou et al. RWMTD - Figure 2

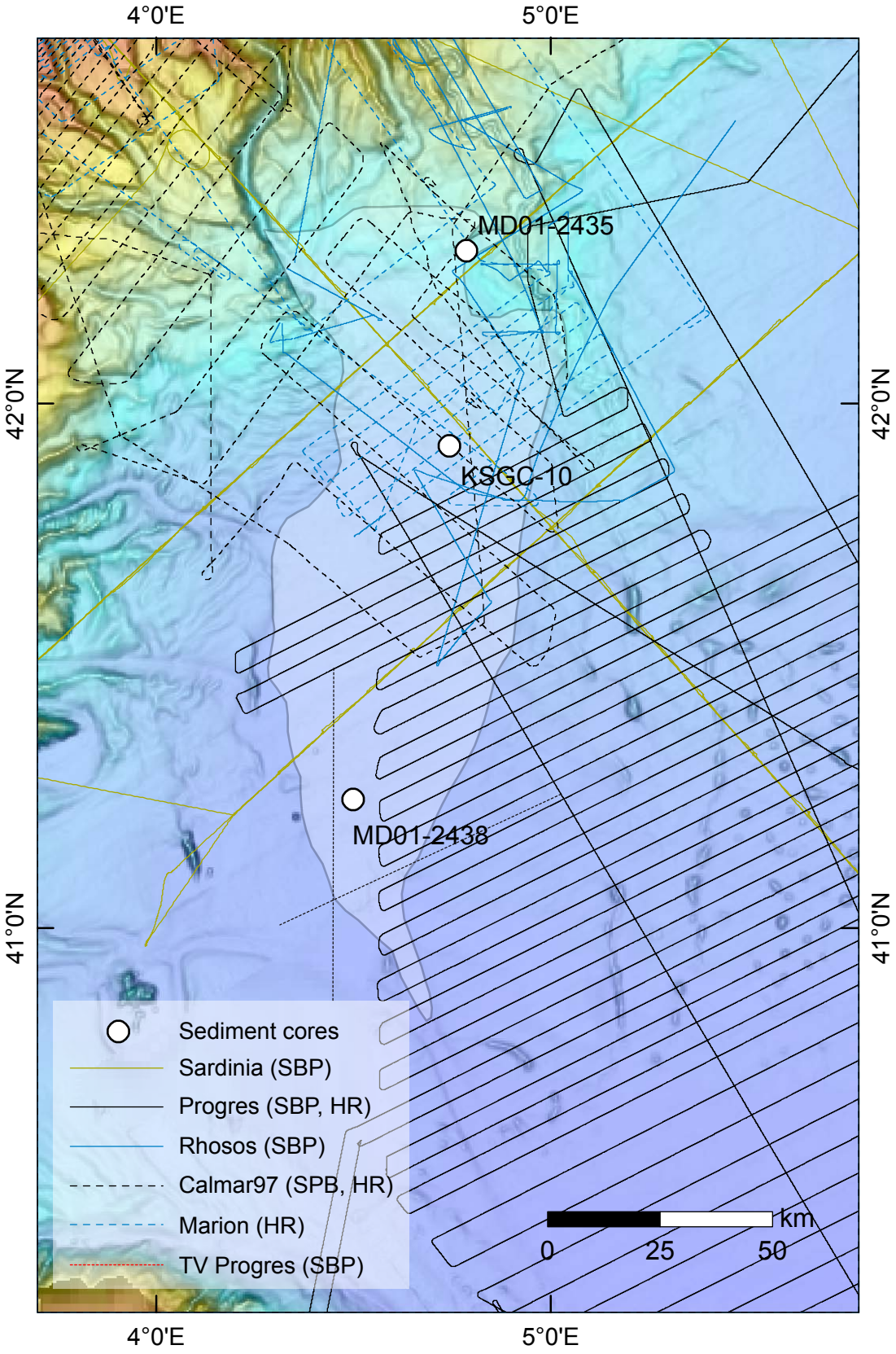

Dennielou et al. RWMTD - Figure 3

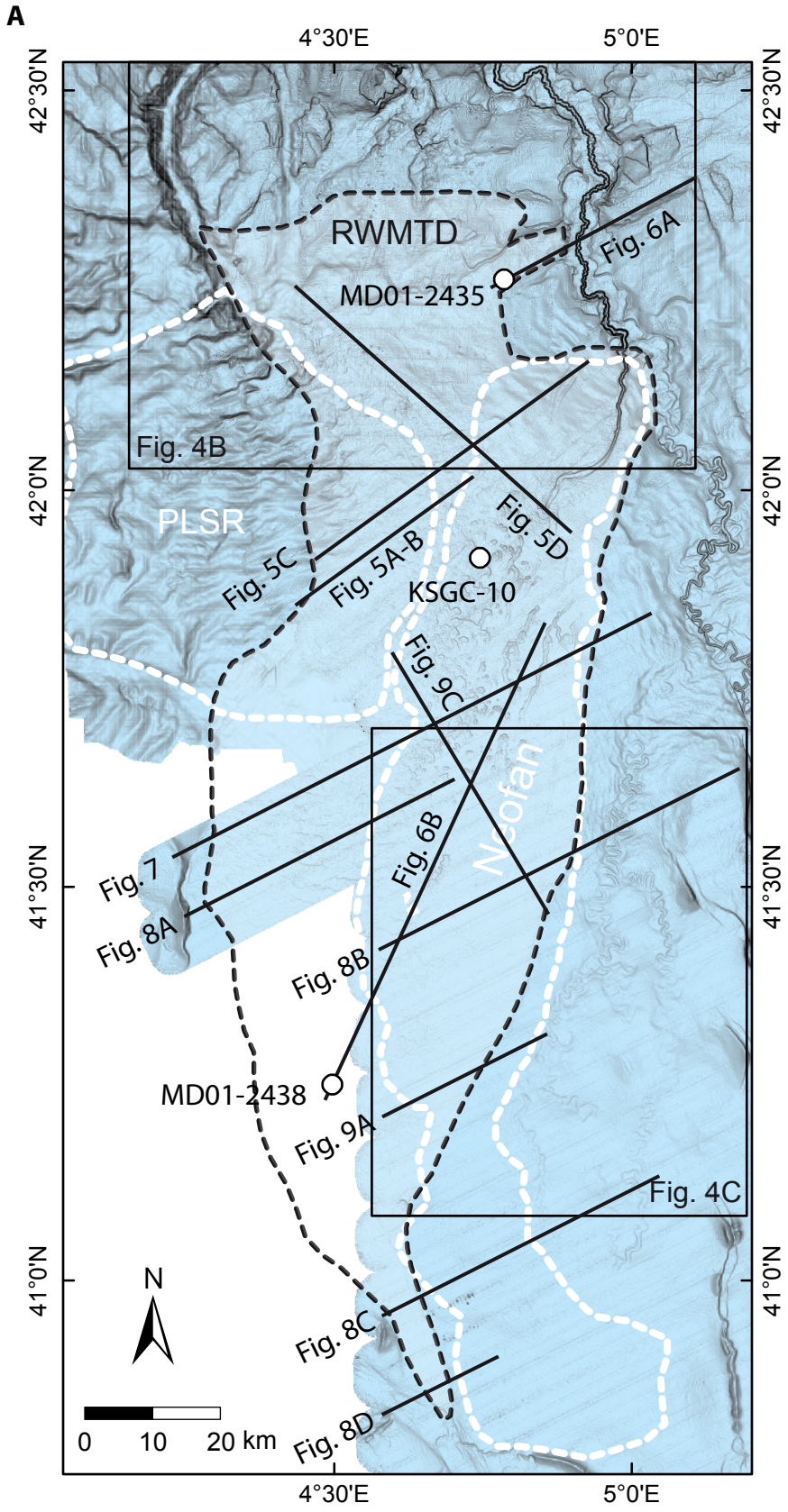

Dennielou et al. RWMTD - Figure 4

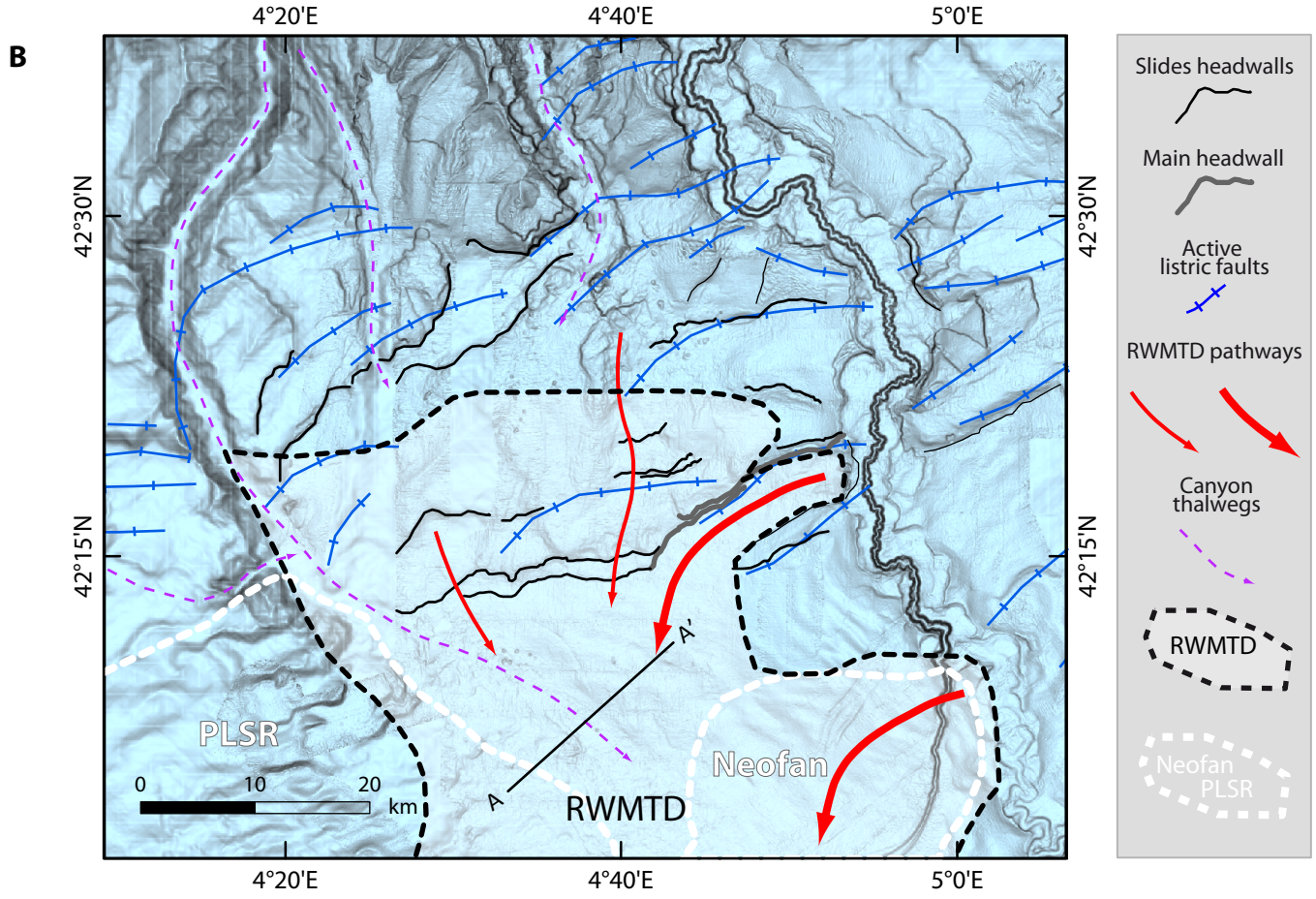

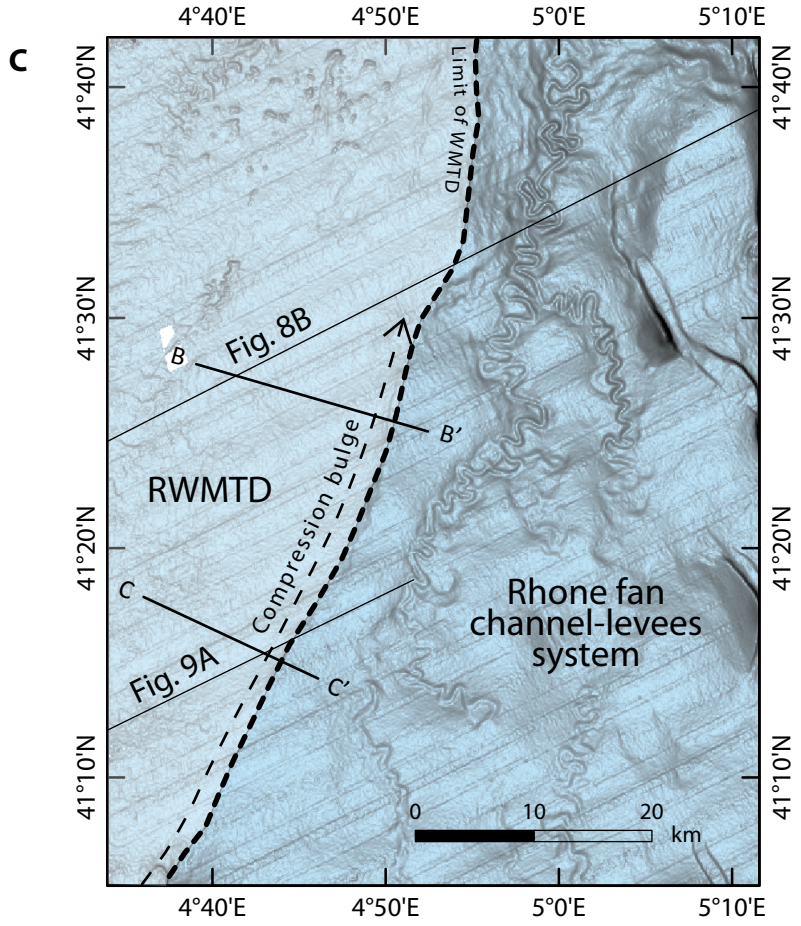

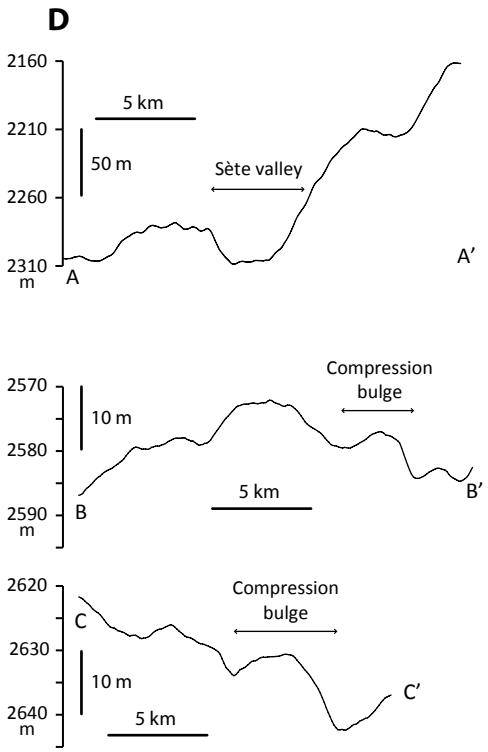

Dennielou et al. RWMTD - Figures 4A, 4B, 4C

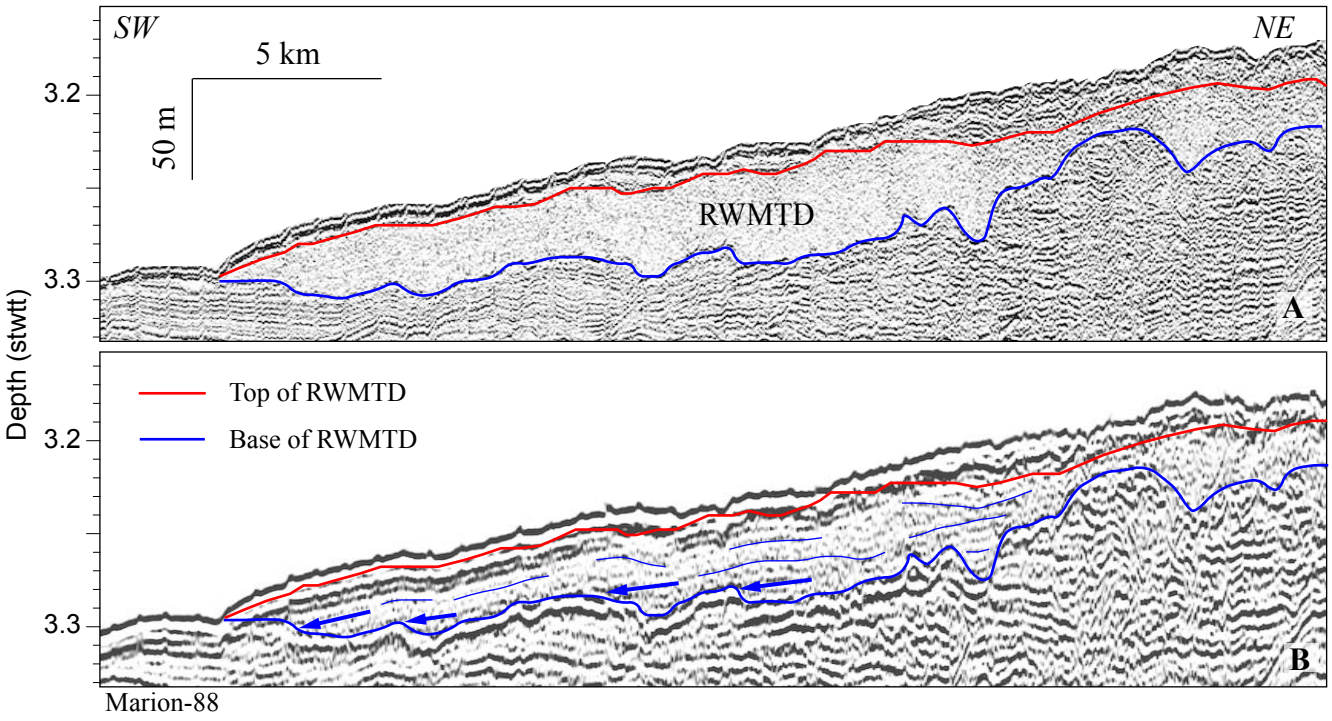

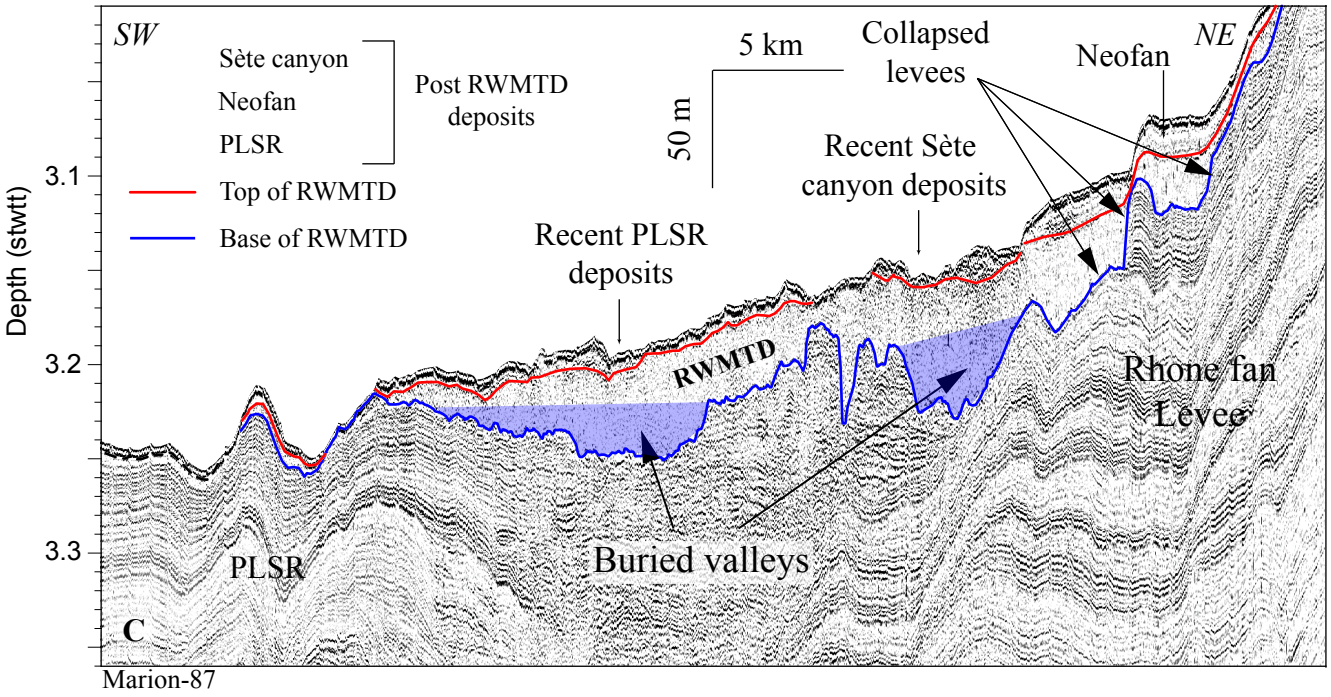

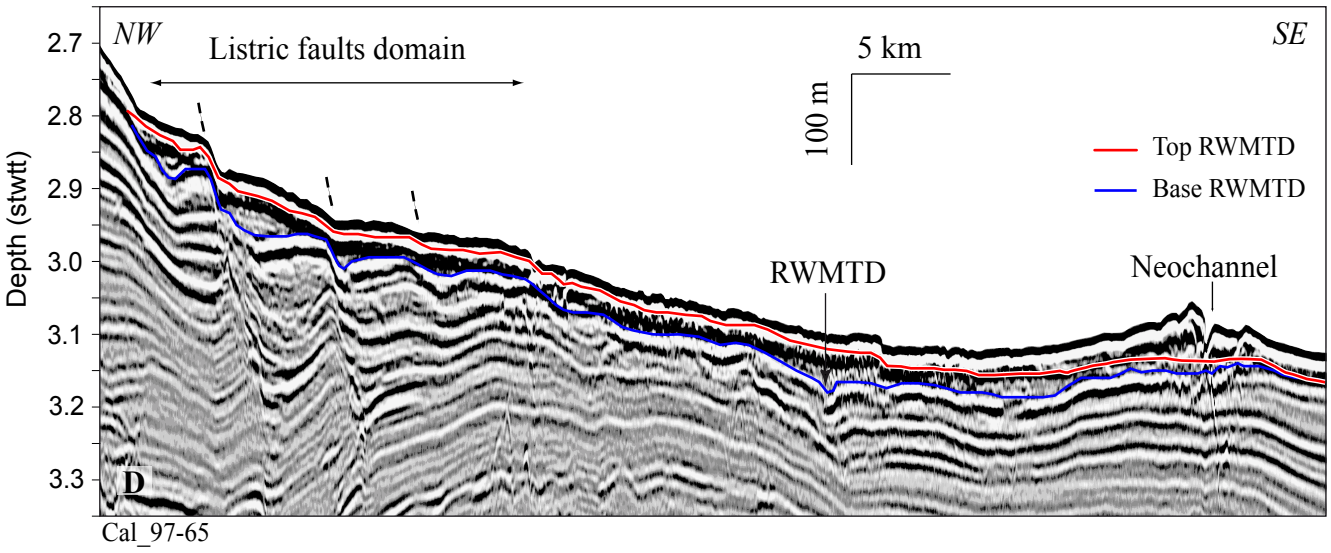

Dennielou et al. RWMTD - Figure 5

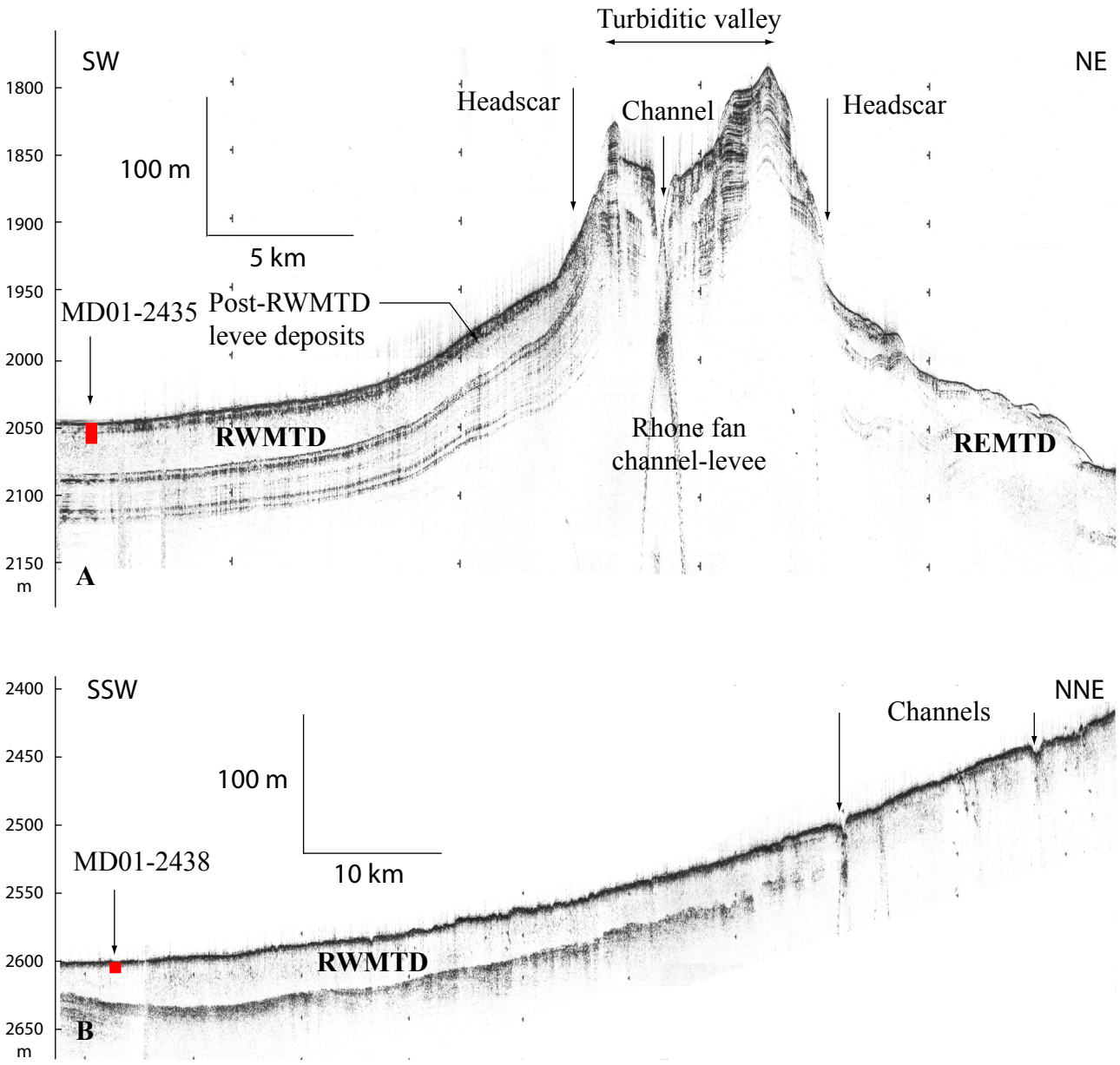

Dennielou et al. RWMTD - Figure 6

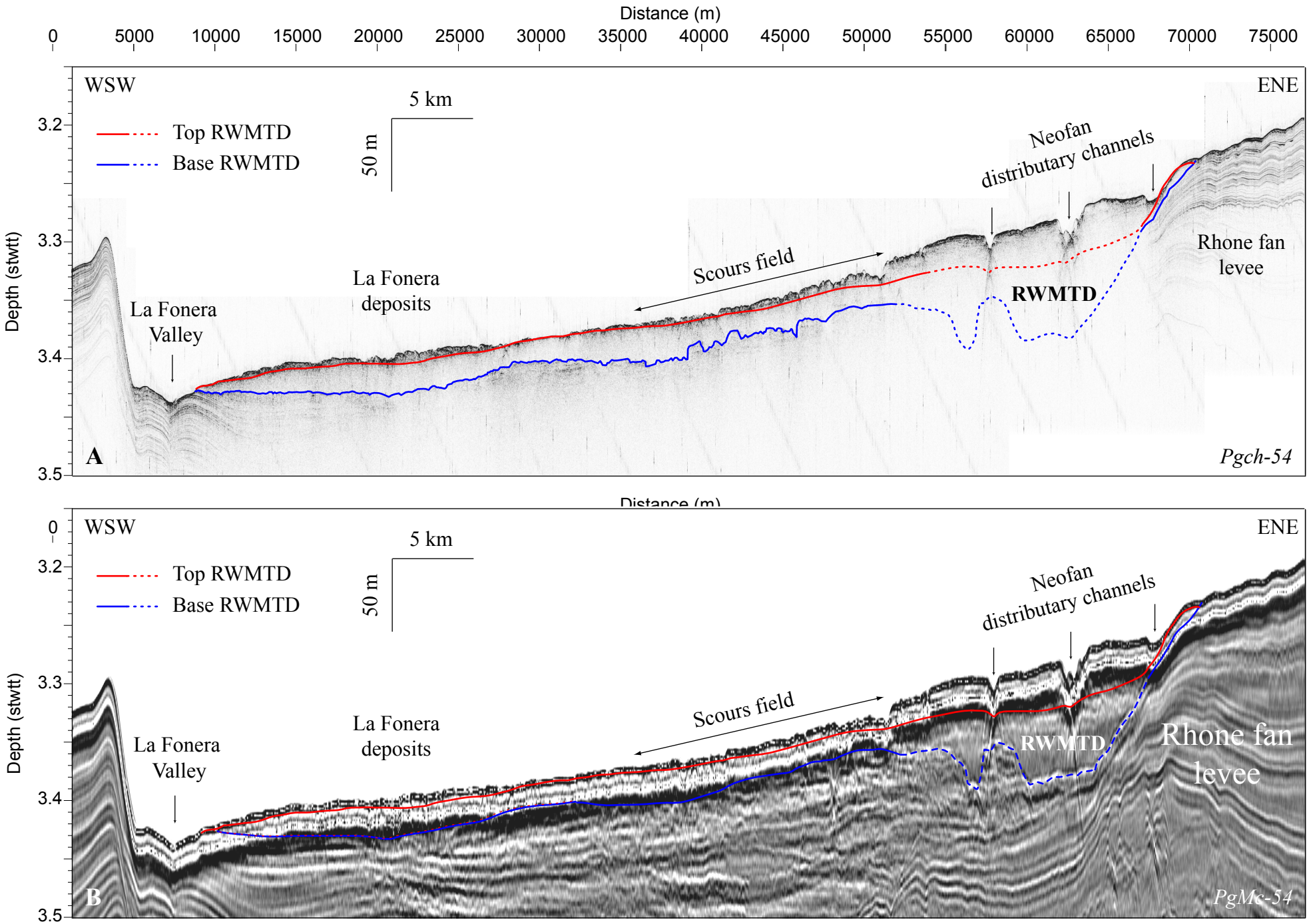

Dennielou et al. RWMTD - Figure 7

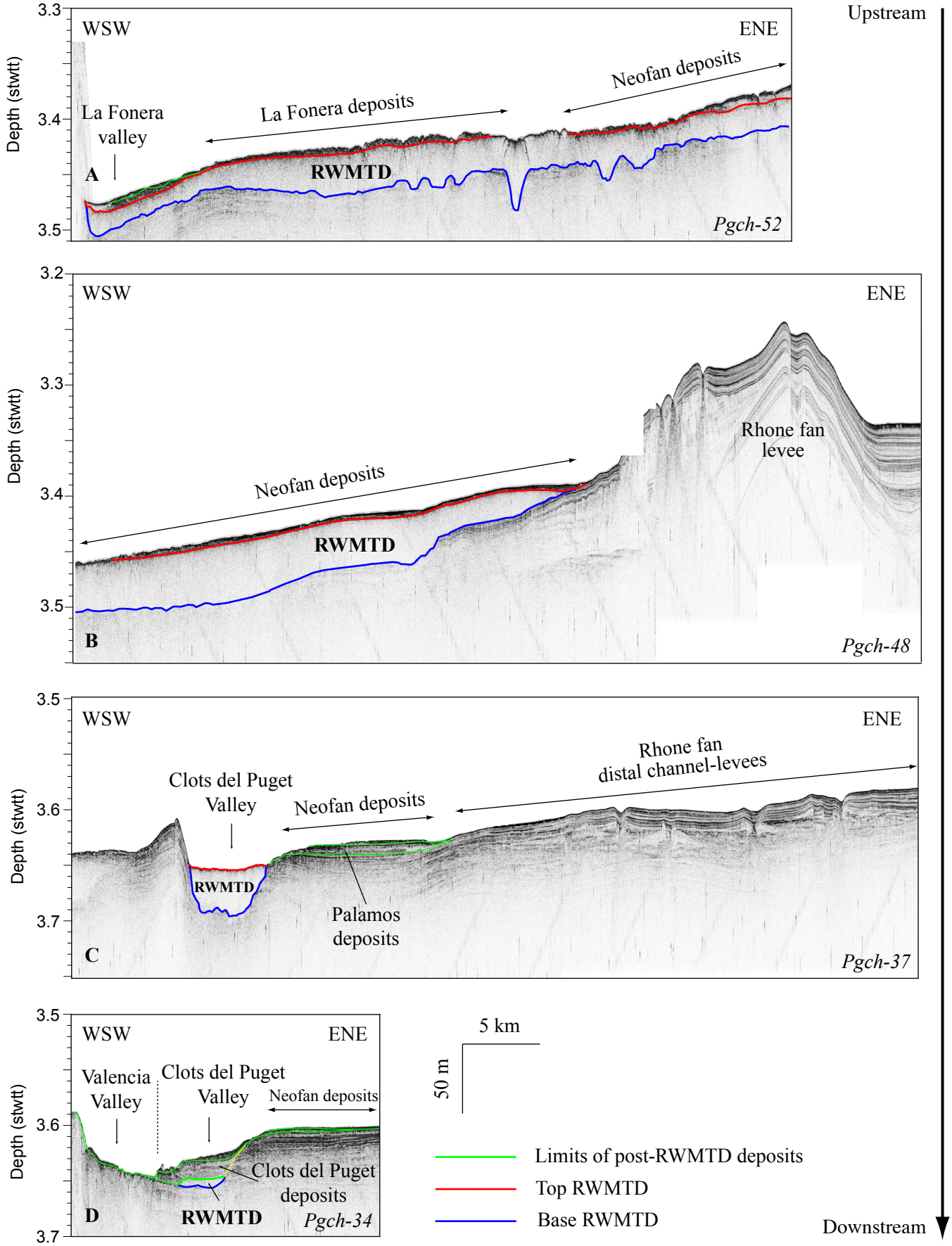

Dennielou et al. RWMTD - Figure 8

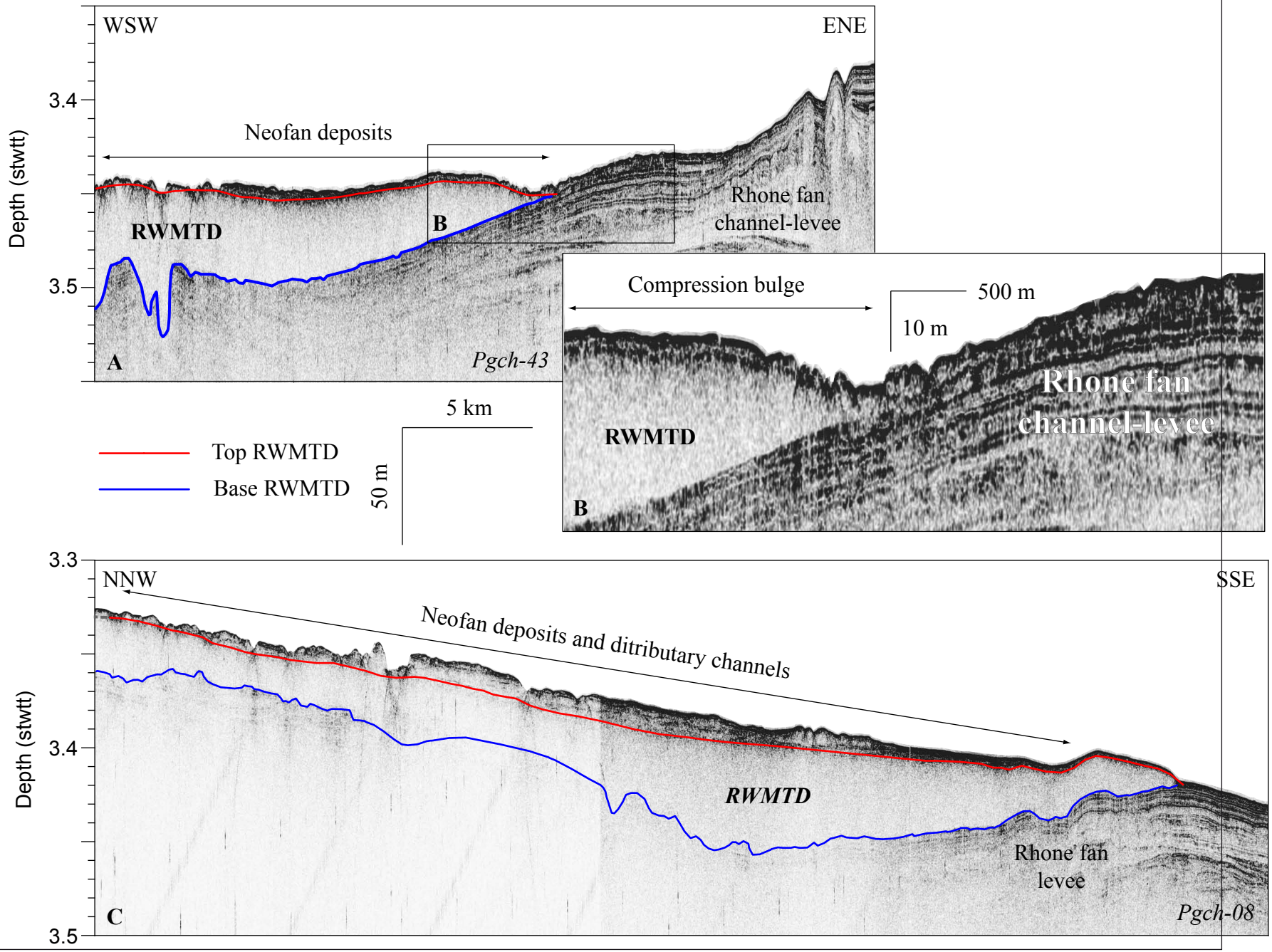

Dennielou et al. RWMTD - Figure 9

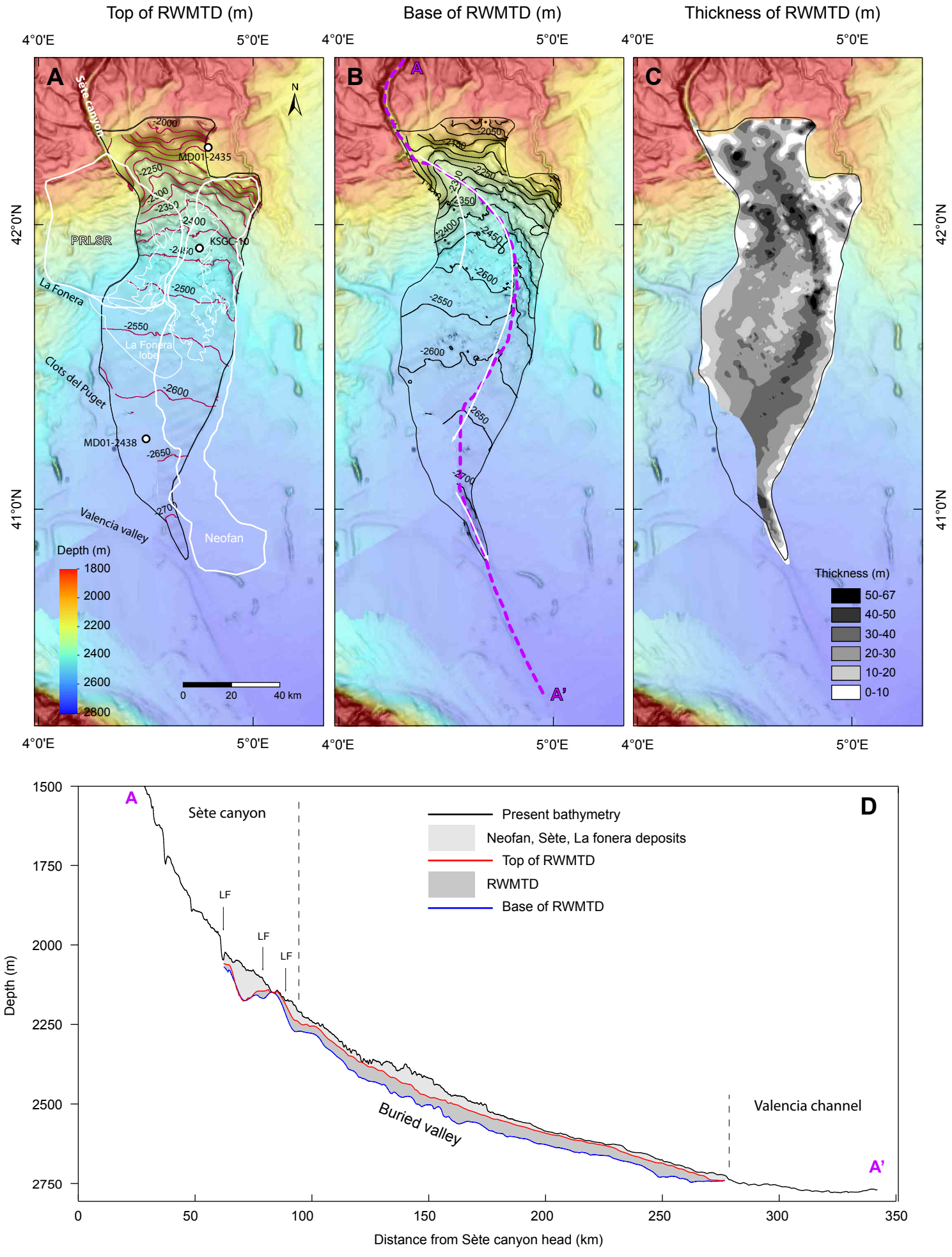

Dennielou et al. RWMTD - Figure 10

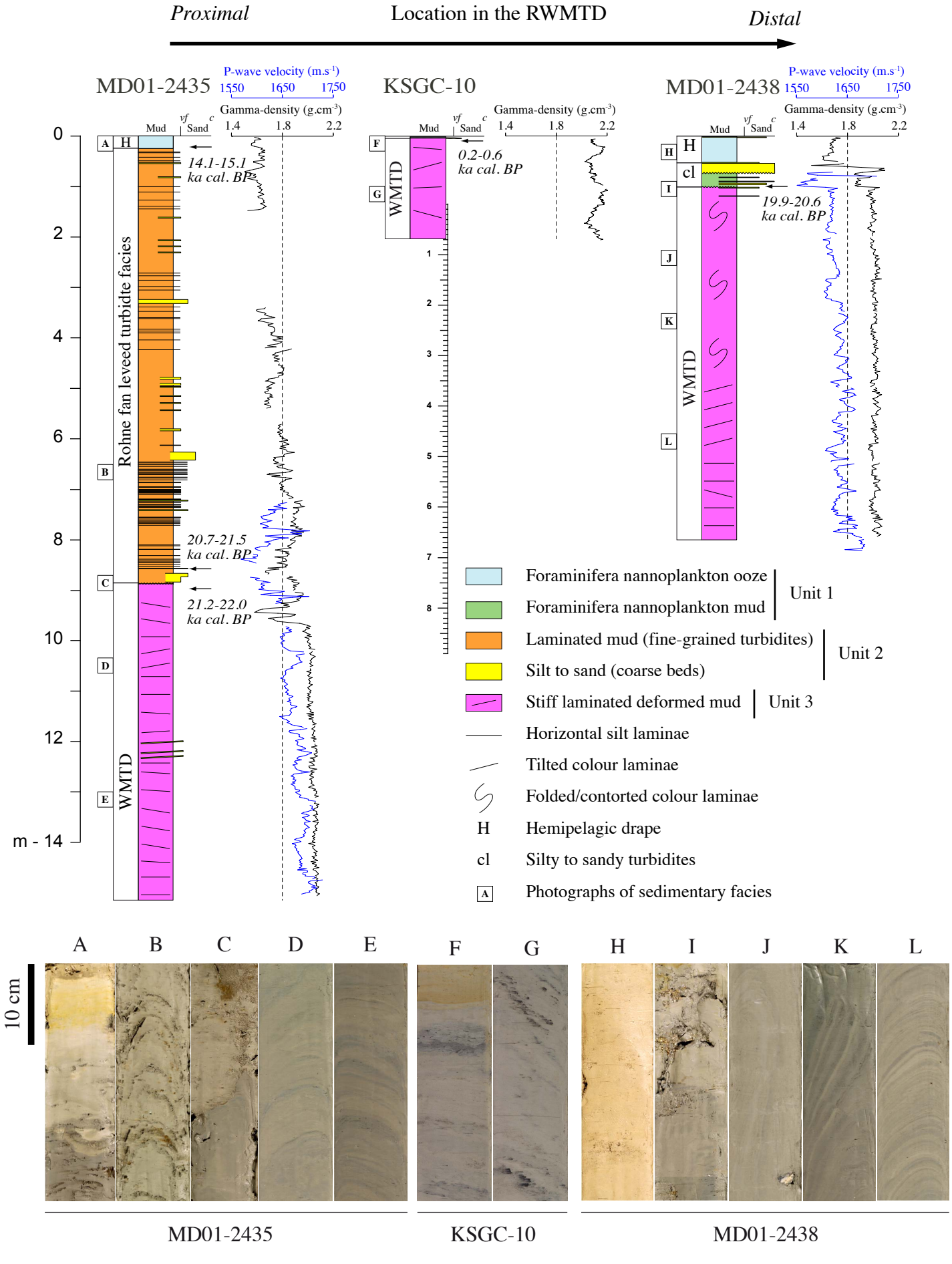

Dennielou et al. RWMTD - Figure 11

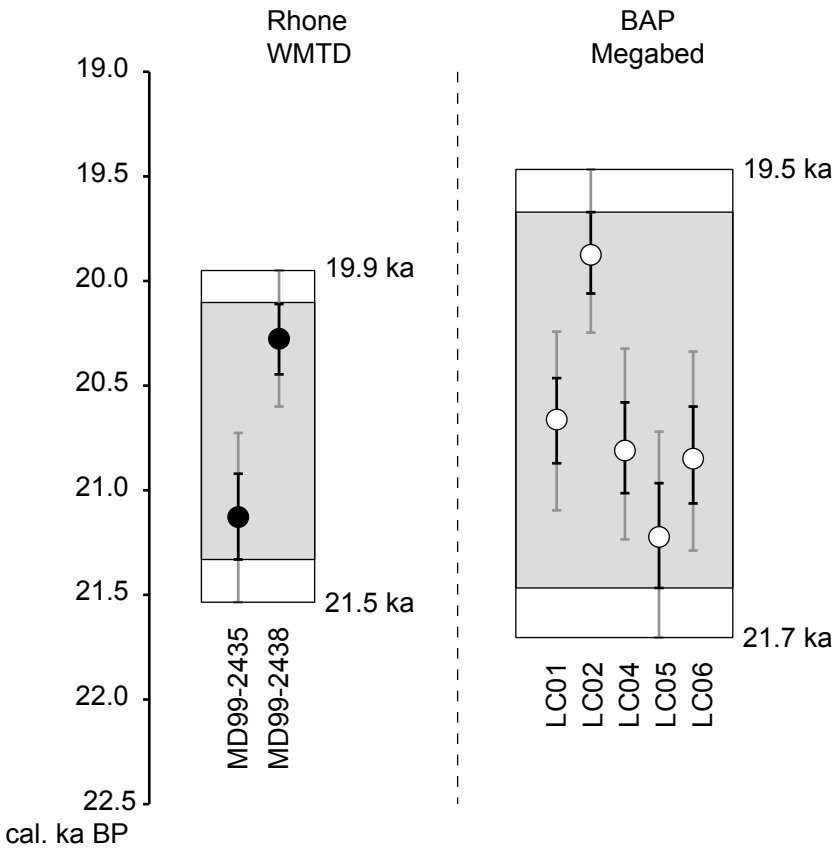

Dennielou et al. RWMTD - Figure 12

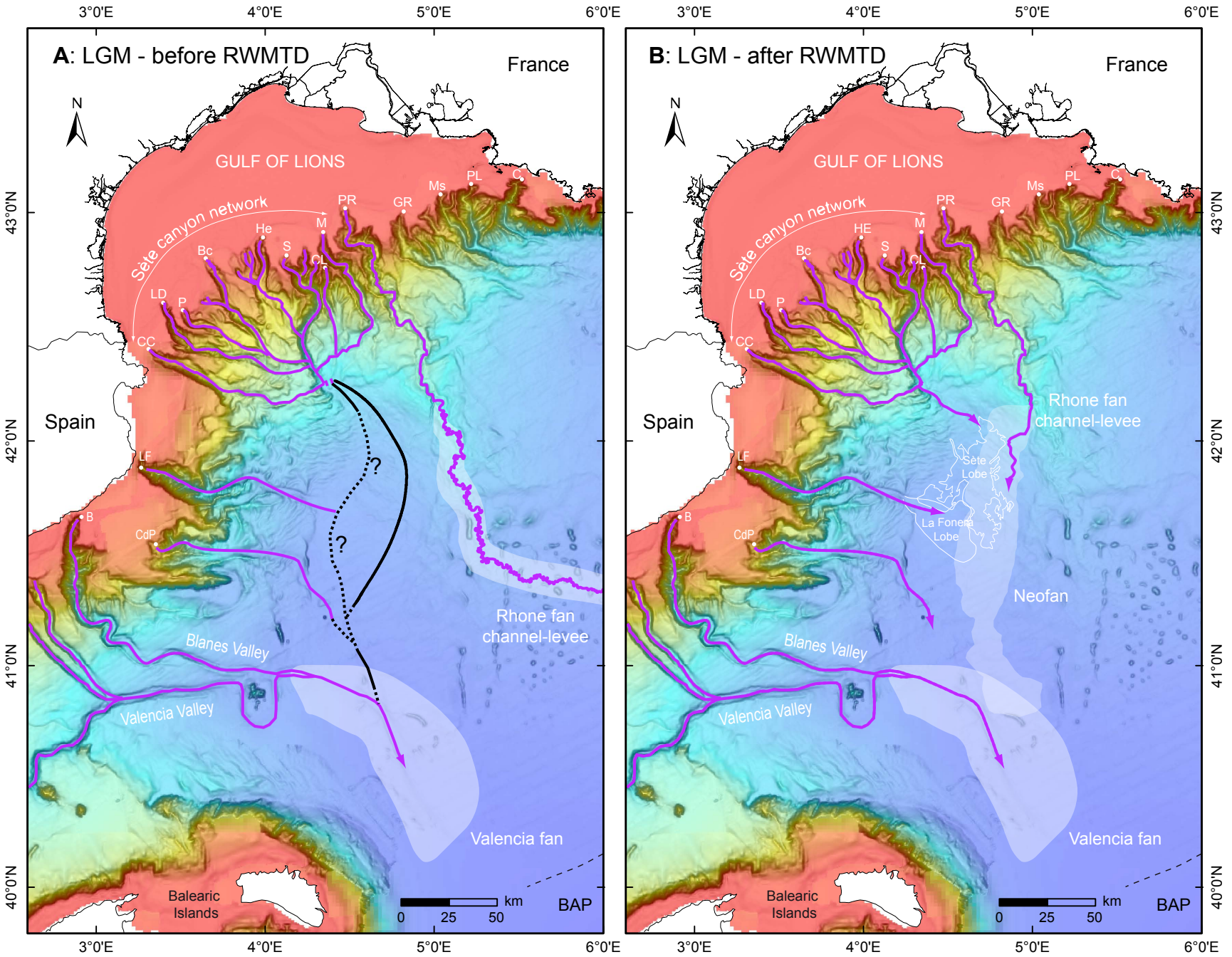

Dennielou et al. RWMTD - Figure 13